Available on the CMS information server **CMS AN-15-021**

CMS Draft Analysis Note

The content of this note is intended for CMS internal use and distribution only

2015/04/05
Head Id: 280085
Archive Id: 283412
Archive Date: 2015/03/10
Archive Tag: trunk

Nuclear Modification Factor RAA of D^0 in PbPb Collisions at $\sqrt{s_{NN}}$= 2.76 TeV

Gian Michele Innocenti, Kurt Jung, Yen-Jie Lee, Stanislav Lisniak, Matthew Nguyen, Jian Sun, Fuqiang Wang, Jing Wang, Ta-Wei Wang, Wei Xie

Abstract

In this analysis note, we present the production cross section and nuclear modification factor RAA of D^0 in Pb-Pb collisions at $\sqrt{s_{NN}}$= 2.76 TeV from CMS

Version notices

V1

- Skeleton is created on Feb. 28th 2015. (Jian)

Contents

1 Introduction

Heavy quarks are dominantly produced by initial hard scatterings and carry clean information from the medium at early stages of the collision because of their large masses. Compared to light quarks, more energy loss mechanisms, e.g. elastic energy loss and collisional dissociation[1], may be involved in heavy-quark interactions with the medium. Detailed measurements of production and correlations for charm and bottom separately may thus provide crucial inputs in understanding the properties of the strongly interacting QCD matter.

In CMS, we observed B hadron suppression in PbPb collisions through non-prompt J/ψ measurements [2] at $\sqrt{s_{NN}}$ = 2.76 TeV. Our measurements of directly reconstructed B meson[3] and B-jet production[4] in pPb collisions at $\sqrt{s_{NN}}$ = 5.02 TeV indicate that the cold nuclear matter effect is not significant. In this note, we present the analysis details of the first CMS measurement of prompt D^0 meson production in 2.76 TeV PbPb collisions. The nuclear modification factor (R_{AA}) is calculated as a function of p_T and N_{part} using the Fixed-Order Next-to-Leading Logarithm (FONLL) calculation [5] as the reference taking into account the B-decay D^0 production estimated from our non-prompt J/ψ measurements.

2 Datasets and Event Selections

2.1 Datasets

This analysis is based on the 150 μb^{-1} of PbPb collisions at $\sqrt{s}$ =2.76 TeV collected by the CMS experiment during the 2011 heavy ion run. A detailed description of the CMS experiment can be found in [6].

2.2 Trigger and event selection

In this analysis, minimum bias trigger "HLT_HIMinBiasHfOrBSC" is used. As described in AN-11-436 [7], Minimum-bias PbPb data are recorded based on coincident signals in the beam scintillator counters (BSC, $3.23 < |\eta| < 4.65$) or in the steel/quartz-fiber Cherenkov forward hadron calorimeters (HF, $2.9 < |\eta| < 5.2$) from both ends of the detector. In order to suppress events due to noise, cosmic rays, double-firing triggers, and beam backgrounds, the minimum-bias trigger used in this analysis is required to be in coincidence with bunches colliding in the interaction region. The trigger has an acceptance of $(98 \pm 2)\%$ for hadronic inelastic PbPb collisions [8].

The event selection cuts used in this analysis are described in detail in previous PbPb notes [9–12] and publications [13–16]. The collected events are cleaned for detector noise artifacts with the use of an HCAL noise cleaning filter, and ECAL spike removal. Events were sorted into different centrality classes. The centrality of heavy-ion interactions, i.e. the geometrical overlap of the incoming nuclei, is related to the number of participating nucleons and hence to the energy released in the collisions. In CMS, the centrality is defined as percentiles of the energy deposited in the HF.

2.3 Signal Monte Carlo

In order to increase the statistics of D^0, D^0 embedded HYDJET samples were produced. QCD events generated by PYTHIA Tune Z2 were filtered by D0 filter and events passing the filter were embedded into a simulated PbPb background generated by HYDJET (version 1.8, tune "Drum"). Around two hundred thousand Pythia+Hydjet events were generated for each bin with $\hat{p}_T$ boundaries of $[0, 15, 30, 50, \infty]$.

The D^0 filter requires that there is at least one D^0 with $p_T > 3\,\mathrm{GeV}/c$, $|\eta| < 2.4$ in the Pythia event. And the D^0 is exclusively decayed to $K\pi$ with EVTGEN [17], in which final state radiations (FSR) is generated using PHOTOS [18].

We are just filtering on D^0 in the simulation production, so the samples produced are inclusive D^0 samples, including prompt D^0 and B feed-down D^0. The fraction of B feed-down D^0 in raw D^0 counts is around 15

3 D^0 reconstruction

In this section, D^0 reconstruction strategy is discussed. In this analysis, D^0 is reconstructed through decay channel D$^0 \rightarrow K^- \pi^+$.

3.1 Track selection

Track collection 'hiGeneralTracks' is used in this analysis. Tracks are required to pass p_T and η cuts, $p_T > 1.5\,\text{GeV}/c$, $|\eta| < 2.4$ and satisfying the track quality cuts listed below:

- Number of hits > 11
- chi2/dof/layer < 0.25
- relative error on $p_T < 7.5\%$

Figure 1 shows the tracking efficiency and fake rate as function of track p_T with track quality cuts above in $|\eta| < 2.4$. The track fake rate is smaller than 2% when track $p_T > 1.5\,\text{GeV}/c$.

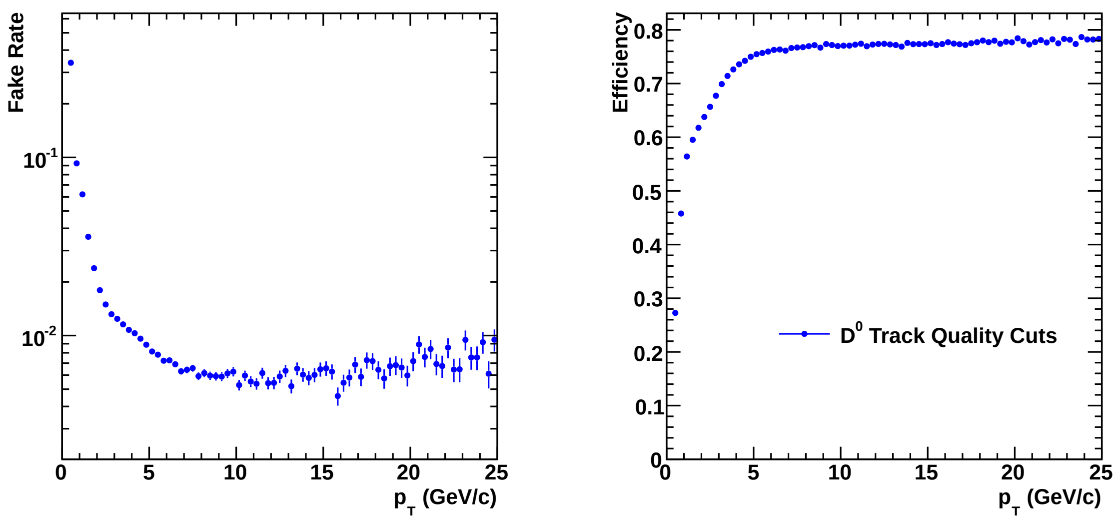

Figure 1: Track fake rate (left) and efficiency as function of track p_T with D^0 track quality cuts in $|\eta| < 2.4$ from QCD DiJet Pthat 80 Embedded HYDJET sample

3.2 D^0 reconstruction

The D^0 candidates are reconstructed by combining pairs of oppositely charged tracks. One of the track is assumed to be K and the other track is assumed to be π. Steps of D^0 reconstruction are as followed:

- Oppositely charged tracks with invariant mass in [1.6648, 2.0648] are selected to form pairs.
- "KinematicParticleVertexFitter" is used to fit the vertex of two tracks.
- Based on the fitted vertex, the decay length d0, decay length error d0error, pointing angle α are calculated, where α is the angle between total momentum vector of tracks and vector connecting primary and D^0 candidate vertex. Cuts are applied to these parameters to increase signal significance as discussed in section 5.1.

4 MC and Data Comparison

In this section, the signal variable comparison between data and simulation is disscussed. To get D^0 signal variable distributions from data, sideband method is used. And to be consistent, sideband method is also used in simulation. Sideband is defined as $100MeV < |M_{D^0} - M_{D^0}^{PDG}| < 150MeV$ and signal region is defined as $|M_{D^0} - M_{D^0}^{PDG}| < 30MeV$. When we do the comparison, distributions from simulation are scaled to the entries of data. Prompt and B feed-down D^0 from simulations are scaled according to the fraction of prompt D^0, which is calculated in Section 7. And prompt D^0 distributions are plottd on the top of B feed-down D^0 distributions to compare with dsitributions from data directly. In data, the signal significance is pretty small if no cuts are applied and we have to apply some cuts to increase the signal background ratio. Cuts applied are d0/d0error > 3.5, $\alpha < 0.05$ and vertex probability > 0.05. Figure 2 shows the comparison for $p_\mathrm{T} > 7.0\,\mathrm{GeV}/c$ D^0. When one variable is studied, cuts on other variables are applied. Red and blue histograms correspond to B feed-down and prompt D^0 components respectively. The plots show that MC and data distributions are in reasonable agreement though statistical error of data is big in some bins.

For $3.5\,\mathrm{GeV}/c < p_\mathrm{T} < 7.0\,\mathrm{GeV}/c$ range, the signal background ratio is pretty small. And we have to apply cuts to all three cut variables to see the D^0 signal peak. Cuts (d0/d0error > 3.5, $\alpha < 0.05$ and vertex probability > 0.05) are applied to make the comparison for D^0 $3.5\,\mathrm{GeV}/c < p_\mathrm{T} < 7.0\,\mathrm{GeV}/c$. Figure **??** shows the varialbe comparisons for $3.5\,\mathrm{GeV}/c < p_\mathrm{T} < 7.0\,\mathrm{GeV}/c$. Again, the plots show MC and data distributions are in reasonable agreement though some differences are observed.

Figure 2 and Figure 3 show the rapidity, d0/d0error, α and vertex probability from data and simulation are in reasonable agreement though differences in some bins are obverserved. Some of the observed differences between data and mc variable distributions are from the unpure signal distributions from data because of the big background. Some difference may also be from the prompt D^0 fraction. And in Section 10, a specific systematic uncertainty due to the remnant discrepancies will be discussed and evaluated.

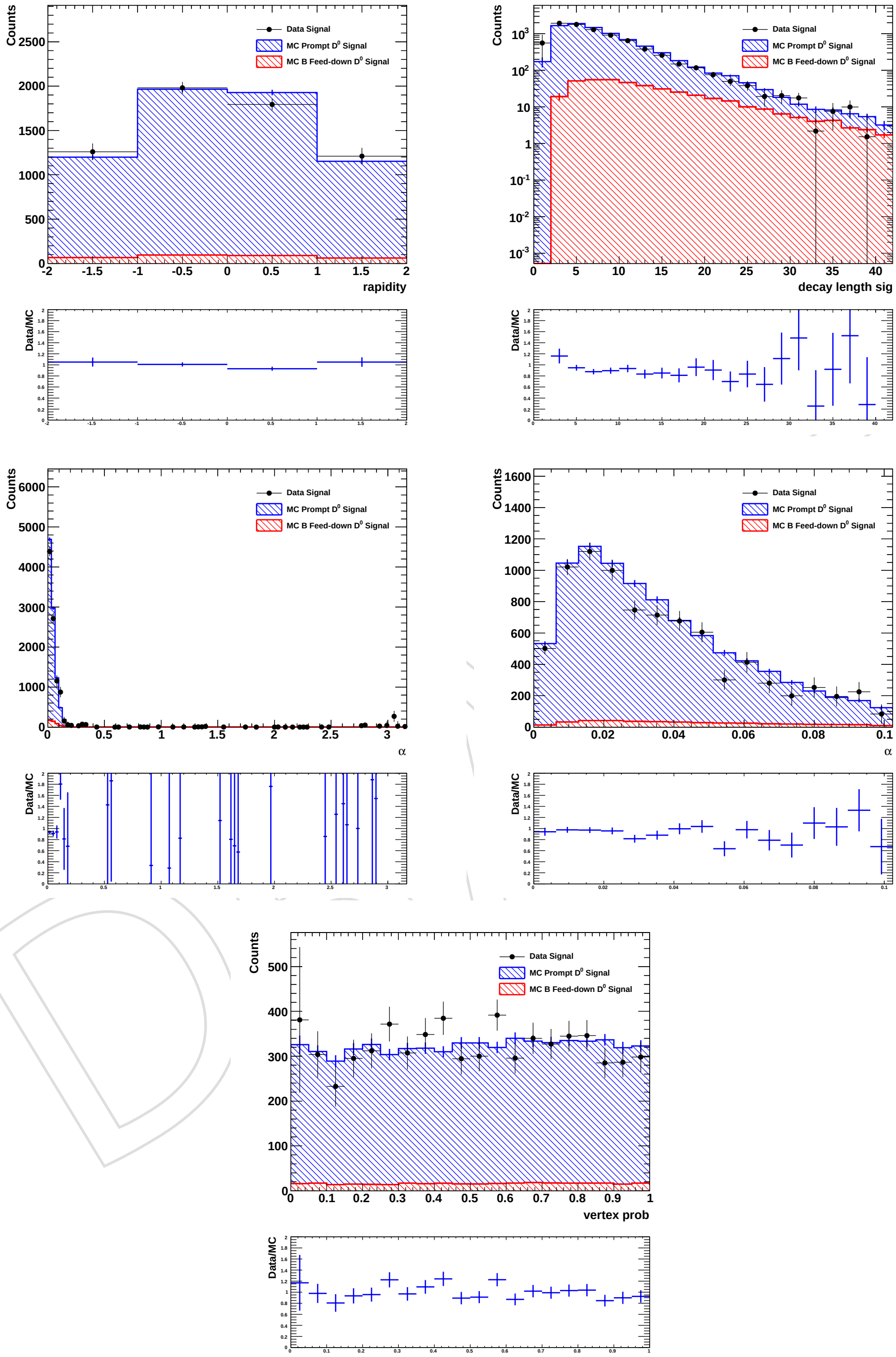

Figure 2: Distributions of rapidity, *d0/d0Err*, α, α zoomed in to range [0, 0.1] and vertex probability for D^0 signals from data and MC simulation with $p_{\mathrm{T}} > 7.0\,\mathrm{GeV}/c$.

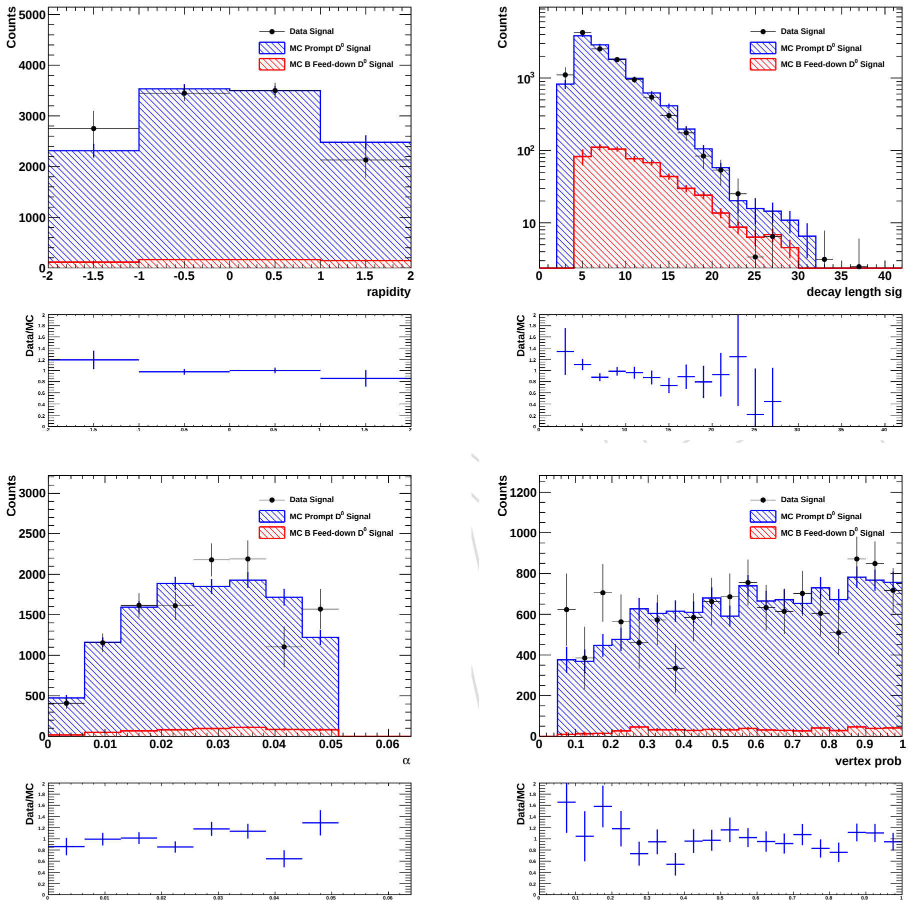

Figure 3: Distributions of rapidity, *d0/d0Err*, α and vertex probability for D^0 signals from data and MC simulation with $3.5\,\mathrm{GeV}/c < p_{\mathrm{T}} < 7.0\,\mathrm{GeV}/c$ with tight cuts applied to all three variables.

5 Signal Extraction

In this section, D^0 candidate and signal yield extraction procedure is described. Optimization of D^0 candidate selection is described in Section 5.1. Signal extraction procedure and the fit results are shown in Section 5.2.

5.1 Cut optimization

The goal of the optimization procedure is to maximize the statistical significance of the signals while keeping reasonably high signal efficiencies. The optimal cut minimizing background efficiency for aspecific signal efficiency is obtained by the TMVA(Toolkit for Multivariate Data Analysis with ROOT) [**?**]. Rectangular cut is chosen as the classification method in TMVA. Reconstructed c andidates which can be matched to generated particles in MC are used as signal sample during training in TMVA, while sideband of data sample is used as background sample. Sideband is defined as 0.1 GeV/c^2 < $|M_{D^0} - M_{D^0}^{PDG}|$ <0.15 GeV/c^2. The amount of background in the signal region is estimated by a linear interpolation using the sideband. Different cut variables are defined for each B meson.

The three selection variables which are common to the three D meson analyses are:

- ffls3d defined as the 3D decay length
- alpha defined as
- prob defined as the probability of D vertex

In Fig. 4, the distributions of the cut variables of signal and background candidates are presented. The optimal cut values are defined as the one maximizing the statistical significance $s/\sqrt{s+b}$. s is the expected number of signal yield from FONLL calculation, multiplied by the MC efficiency and acceptance, and b is the expected number of background in the signal region. Signal region is defined as $|M_{D^0} - M_{D^0}^{PDG}| < 2\sigma$. σ is the width of D candidates mass fitting in MC. Fig. 5 presents the values of the significance versus the signal efficiency. How to get s and b is explained in detail below and Fig. 6 shows the example of definition of signal and sideband region for .

- $s = s' \times$ (signal cut efficiency) where s′ is the number of D candidate in data before cuts and signal cut efficiency is D candidate after optimal cuts over D candidate before optimal cuts. $s' = sT\times$ (pre-filter efficency) where sT is expected number of D meson from FONLL expectation and pre-filter efficiency is the ratio of (reconstructed B candidate after pre-cuts in MC) over (generated candidate number in MC).
- $b = b' \times$ (background cut efficiency) where b′ is the number of D candidate in data before cuts and background cut efficiency is D candidate after optimal cuts over D candidate before optimal cuts. $b' = b_{sideband} \times (width_{signal\ region}/width_{sideband})$ where sideband is defined as $0.1 < |M_B - M_B^{PDG}| < 0.15$ GeV/c^2.

The final cut values are reported in Table 1.

5.2 Signal Extraction and D^0 Raw Yield

Raw yields are extracted in each p_T-interval via a fit procedure. The fit functions (PDF to model the mass spectrum) consists of a Gaussian for the signal and a PDF that describes the background shape. The PDF of describing the background shape can be polynomial or exponential. For default fit, second order polynomial is used as background PDF. Exponential is used as background PDF to estimate the systematic uncertainty of signal extraction in Section 10. In addition, there is no PID on each single track, so K and π tracks from real D^0 may form two D^0

p_T	**ffls3d**	**alpha**	**fprob**
4.5-5.5	> 3.98	< 0.065	> 0.082
5.5-7.0	> 4.14	< 0.069	> 0.209
7.0-9.0	> 3.87	< 0.053	> 0.113
9.0-11.0	> 4.36	< 0.066	> 0.093
11.0-13.0	> 3.68	< 0.075	> 0.057
13.0-16.0	> 3.59	< 0.060	> 0.107
16.0-20.0	> 3.25	< 0.061	> 0.025
20.0-28.0	> 2.76	< 0.055	> 0.068
28.0-40.0	> 3.18	< 0.133	> 0.022

Table 1: Summary table of the topological cut values.

candidates (Kπ and πK). Figure 7 shows fitted D^0 mass spectrum from simulation. And it is clear that the gray open circles, which stand for the D^0 candidates with wrong particle identity assigned to daughter tracks (should be Kπ, but assigned as πK), has a pretty broad mass distribution compared with the real D^0 (pink open circles) and the mass shape can be described well by second order polynomial. And the Gaussian compontent (pink dashed lines) of the fit results match the MC Truth D^0 candidates pretty good. The particle misidentification is studied as a specific systematic error in Section 10.

The raw yields are extracted by fitting the D^0 candiate mass spectrum with the fit functions composed of a Gaussian and a second order polynomial as discussed above. The fit ranges in most p_T bins are [1.7 GeV, 2.05 GeV] and tuned in some specific p_T bins to get better fit results. In Figure 8 , the fits to D^0 candidate mass distribution in different p_T bins $|y| < 2.0$ and centrality $0-100\%$ are presented. And in Tab. 2, the values of the raw yields extracted in each p_T bins are reported togetheer with the mean and the width of the signal shapes.

p_T(GeV/c)	**Mass mean(MeV/c^2)**	**Mass error(MeV/c^2)**	**Signal extracted**	**Signal extracted error**
$3.5-4.5$	1864.14	13.39	5031.2	$\pm$483.7
$4.5-5.5$	1863.64	11.33	3874.5	$\pm$264.2
$5.5-7$	1863.01	13.57	3790.2	$\pm$186.0
$7-9$	1865.14	14.88	2630.4	$\pm$114.7
$9-11$	1864.90	14.48	1346.5	$\pm$72.0
$11-13$	1865.12	14.32	973.6	$\pm$58.0
$13-16$	1864.19	12.61	600.7	$\pm$41.4
$16-20$	1864.11	12.61	410.2	$\pm$37.8
$20-28$	1862.26	16.25	263.6	$\pm$34.4
$28-40$	1869.80	17.01	90.9	$\pm$22.2

Table 2: Summary table of the signal extracted of D^0 with $|y| < 2.0$ and centrality $0-100\%$. Signal extracted error is only statistical.

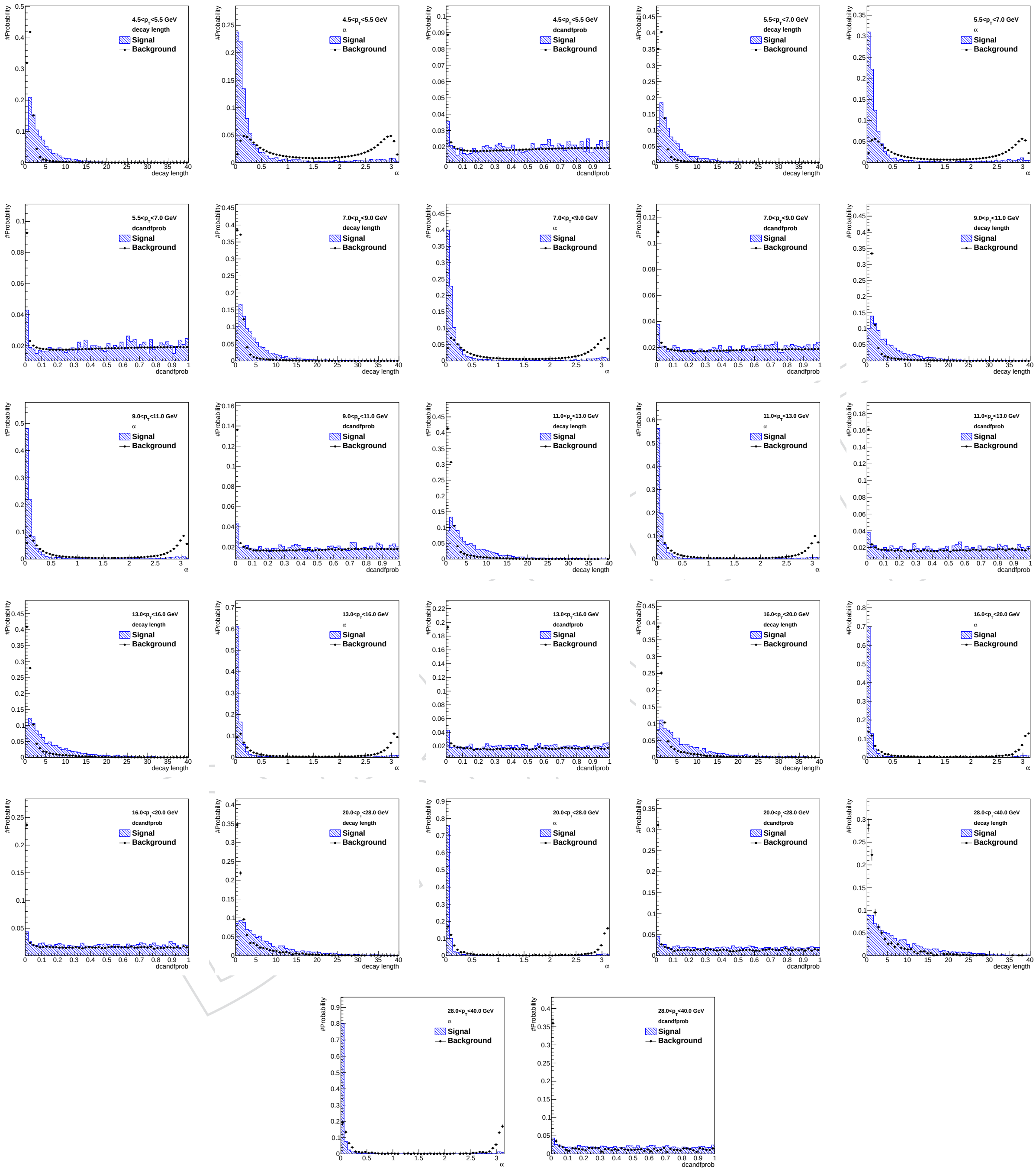

Figure 4: Distributions of D^0 cut variables for background and signal candidates.

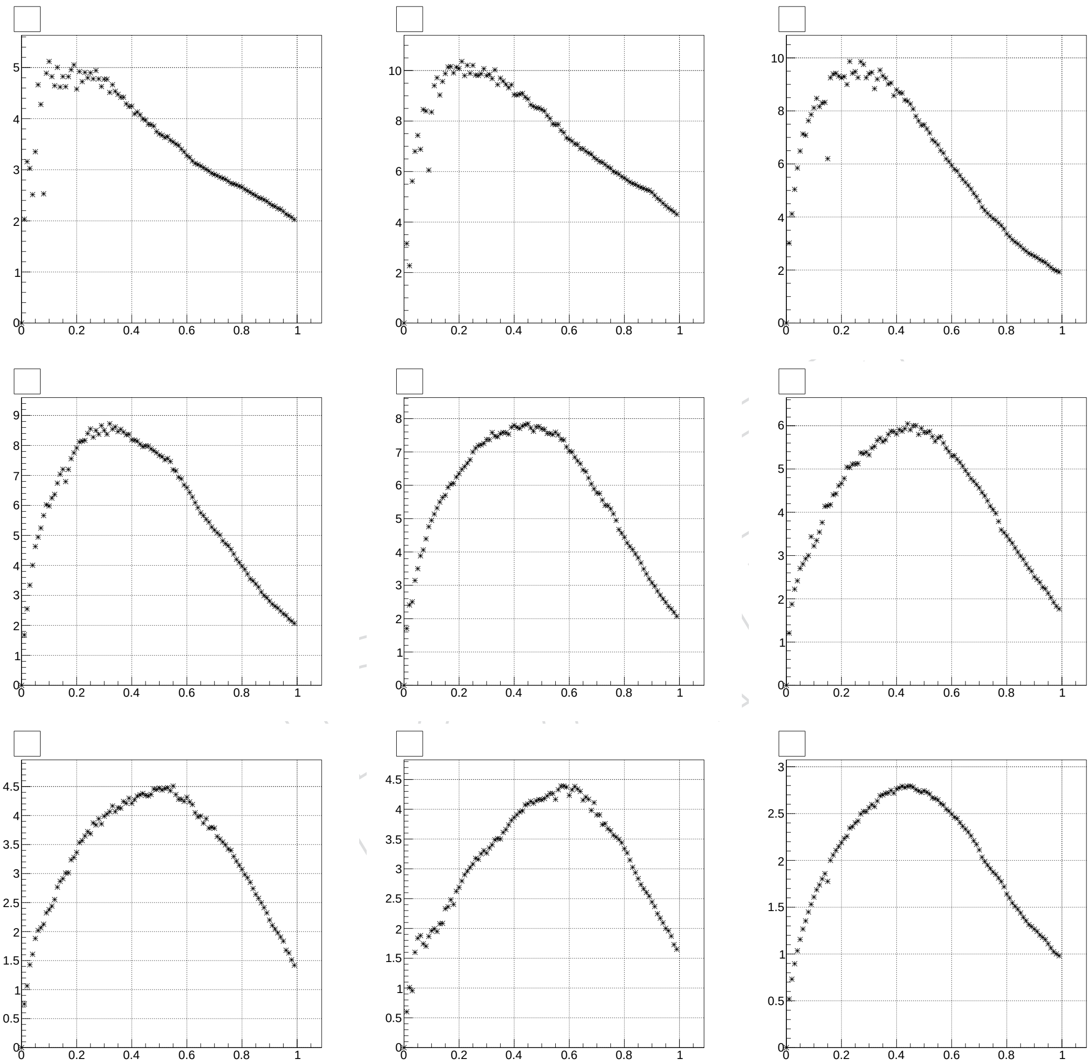

Figure 5: Statistical significance versus signal efficiency. Significance is defined as $s/\sqrt{s+b}$.

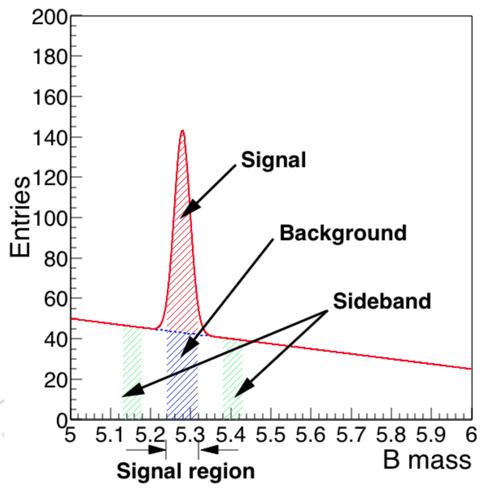

Figure 6: Example of signal and sideband region for significance study for D^0, where signal and sideband region are defined as $|M_{D^0} - M_{D^0}^{PDG}| < 2\sigma$ and $0.1 < |M_{D^0} - M_{D^0}^{PDG}| < 0.15$ GeV/c^2, respectively.

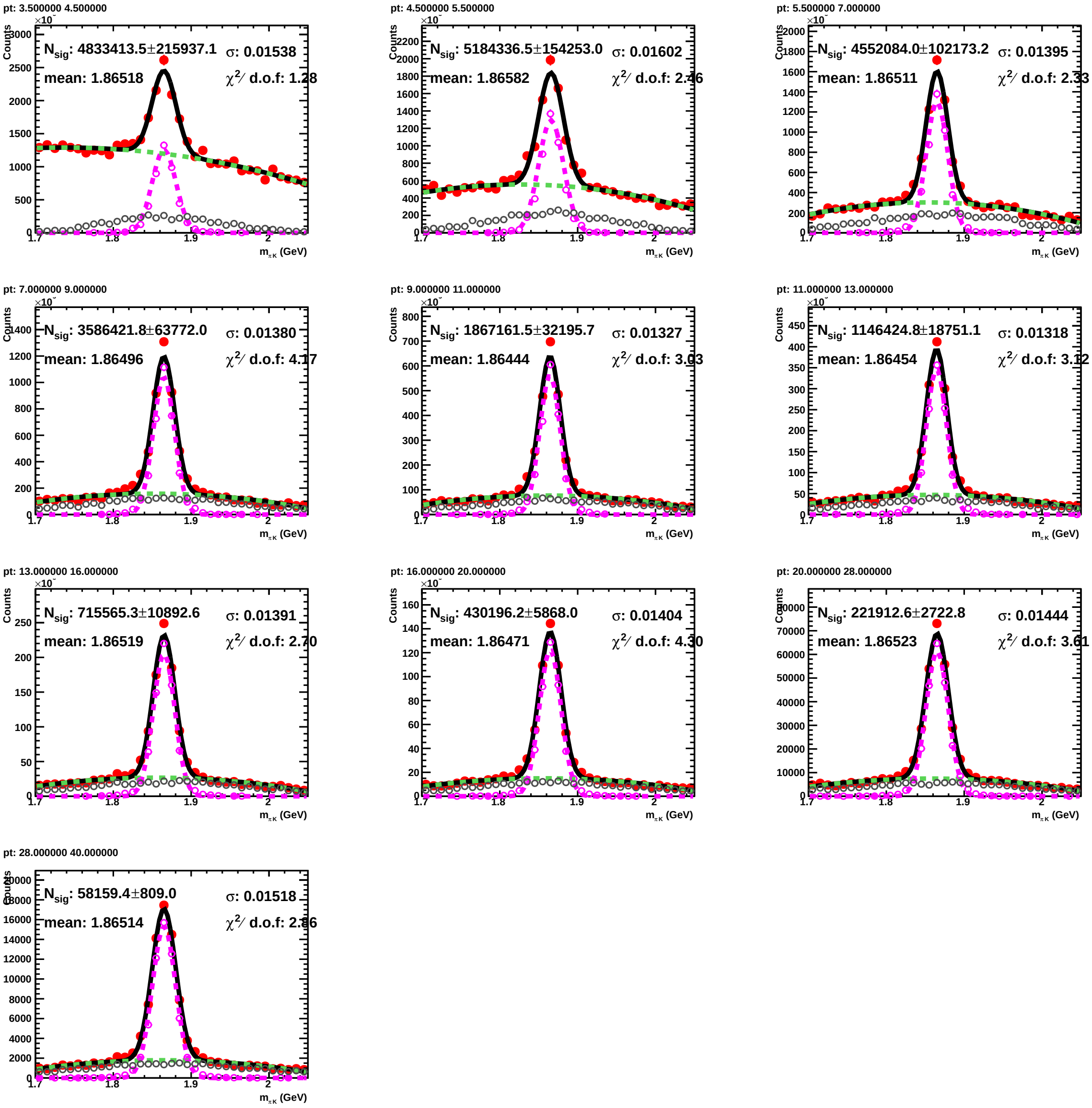

Figure 7: Invariant mass fit of D^0 candidates in bins of D^0 p_T from simulation, $|y| < 2.0$ and centrality $0 - 100\%$. Red points are all D^0 candidates. Black lines are the fit results. Pink dashed lines are Gaussian compontent of the fit results. Green dashed lines are the second order polynomial compontent of the fit results. Pink open circles are MC Truth D^0 candidates. Gray open circles are D^0 candidates with daughter tracks misidentification.

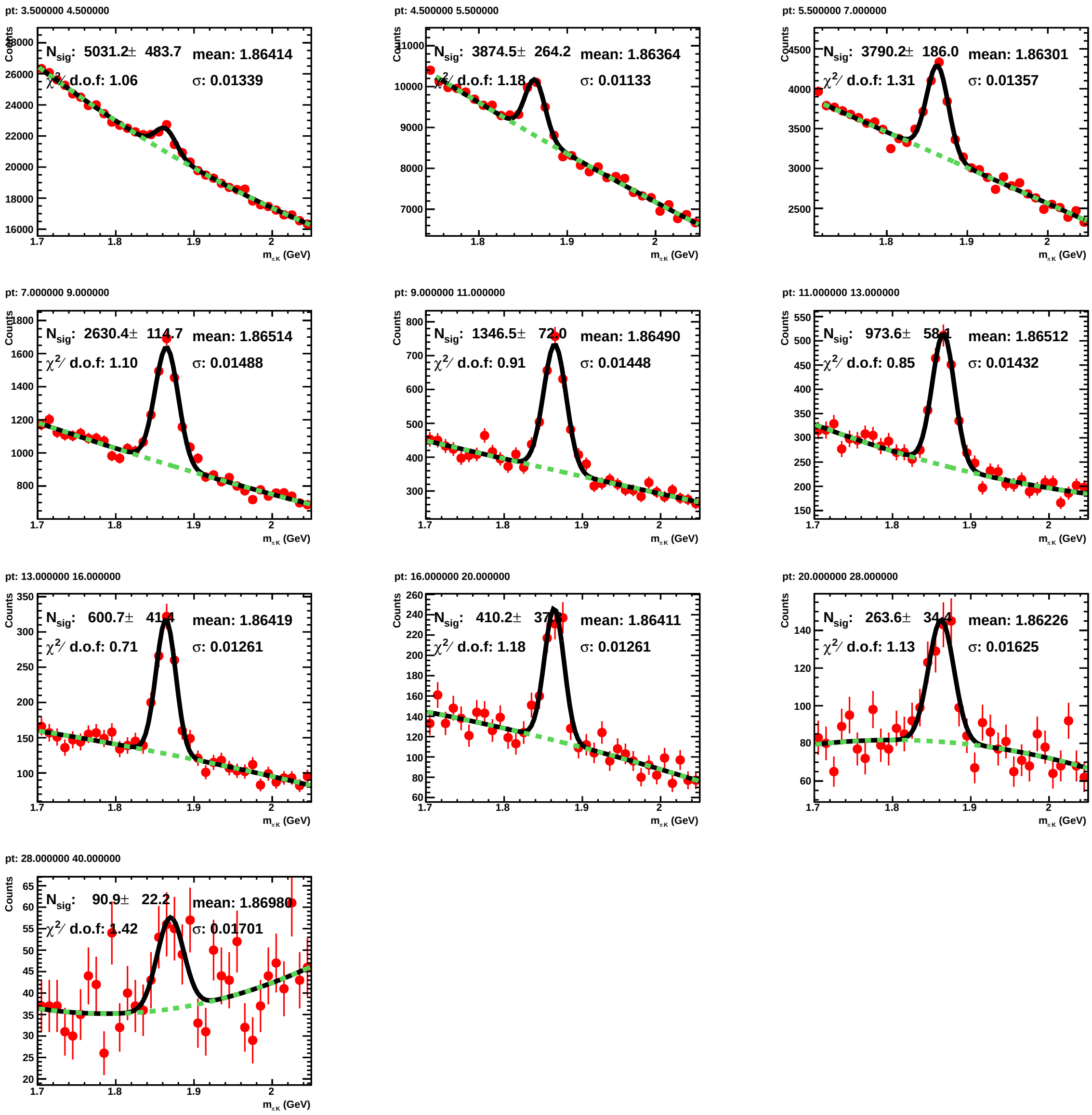

Figure 8: Invariant mass fit of D^0 candidates in bins of D^0 p_T in data, $|y| < 2.0$ and centrality $0 - 100\%$.

6 Acceptance and Efficiency correction

Corrections to the measured spectra can typically be factorised into acceptance(α) $\times$ efficiency(ϵ) corrections, the latter being the product of reconstruction and selection efficiency. We compute the overall correction directly from simulated D^0 embedded in HYDJET 1.8 (Drum tune), which is discussed in Section 2.3. Section 6.0.1 shows the acceptance times efficiency. For deeper understanding and cross-check, efficiency corrections are split in acceptance $\times$ reconstruction efficiency and D^0 cuts selection efficiency. The correction factors are calculated for prompt D^0 and B feed-down D^0 respectively. In the correction factor calculation, MC Truth Candidate, which means D^0 candidates matching to generated D^0 and the matching procedure is described in Section 6.0.4, is used.

To calculate the correction factors, the generated D^0 pt spectrum is weighted to FONLL D^0 spectrum. The weight is done to prompt and B feed-down D^0 respectively. FONLL prompt D^0 spectrum is discussed in Section 8 and FONLL B feed-down D^0 spectrum is discussed in Section 7. In addidtion, D^0 from different pthat events may have slightly different correction factors because different surroundings may affect the reconstruction performance. Thus we also tried to weight the different pthat samples with crosssection and filter efficiency to get the correction factors as discussed in Section 10 and a specific systematic error is assigned to the difference.

6.0.1 Acceptance $\times$ Efficiency

Corrections of acceptance and efficiency can be estimated as a whole from the D^0 embedded HYDJET samples. The idea is to devide the number of MC Truth D^0 candidates by the number of initially generated D^0, one accesses $\alpha \times \epsilon_{reco+cuts}$ as a whole. The formula used is the following:

$$\alpha \times \epsilon_{reco+cuts}(p_T, y) = \frac{N^{MC\ Truth\ Candidate}_{|y|<2.0, p_T^{dau\ track} \geq 1.5, |\eta^{dau\ track}|<2.4, all\ track\ quality\ cuts, all\ D^0\ cuts}}{N^{gen}_{|y|<2.0}} \quad (1)$$

where $N^{MC\ Truth\ Candidate}_{|y|<2.0, p_T^{dau\ track} \geq 1.5, |\eta^{dau\ track}|<2.4, all\ track\ quality\ cuts, all\ D^0\ cuts}$ and N^{gen} are the numbers of reconstructed and generated D^0 respectively.

Figure 9 and Figure 10 respectively show the $\alpha \times \epsilon$ corrections of prompt D^0 and B feed-down D^0 as a function of p_T and y in centrality 0-100%. This is also done in centrality bins studied as showed in Figure.

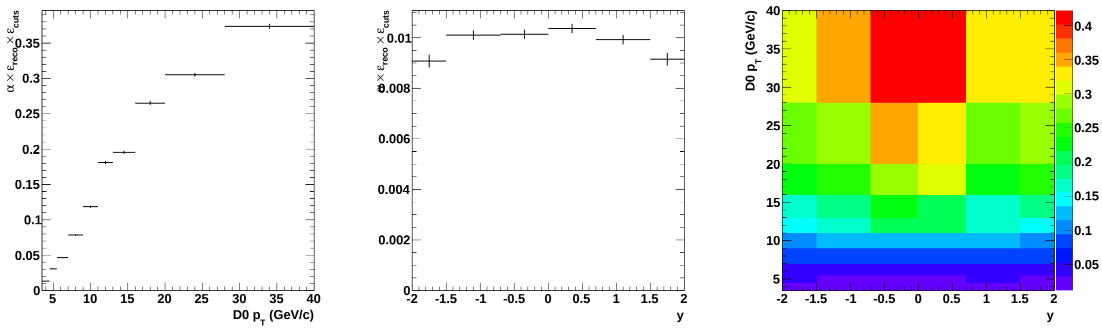

Figure 9: $\alpha \times \epsilon_{reco+cuts}$ of prompt D^0 as function of pt and y

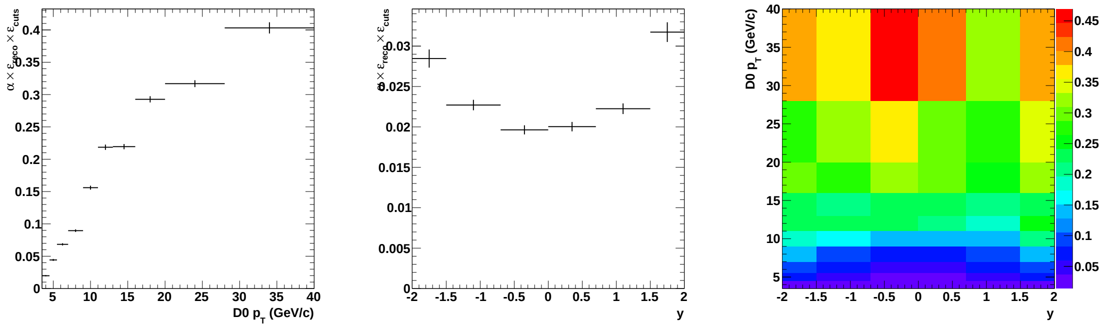

Figure 10: $\alpha \times \epsilon_{reco+cuts}$ of B feed-down D^0 as function of pt and y

6.0.2 Acceptance × Reconstruction Efficiency

This subsection provides the estimation of $\alpha \times \epsilon_{reco}$, which includes effect from the detector accpetance and tracking. The formula used is the following:

$$\alpha \times \epsilon_{reco}(p_T, y) = \frac{N^{MC\ Truth\ Candidate}_{|y|<2.0, p_T^{dau\ track} \geq 1.5, |\eta^{dau\ track}|<2.4, all\ track\ quality\ cuts, no\ D^0\ cuts}}{N^{gen}_{|y|<2.0}} \tag{2}$$

Figure 11 and Figure 12 respectively show the $\alpha \times \epsilon_{reco}$ of prompt D^0 and B feed-down D^0 as a function of p_T and y in centrality 0-100%. This is also done in centrality bins studied as showed in Figure. As you can see from the plot, $\alpha \times \epsilon_{reco}$ of B feed-down D^0 is lower than that of prompt D^0. It is because tracks from B feed-down D^0 are more displaced than tracks from prompt D^0 and Hi Tracking has better performance with tracks closer to primary vertex.

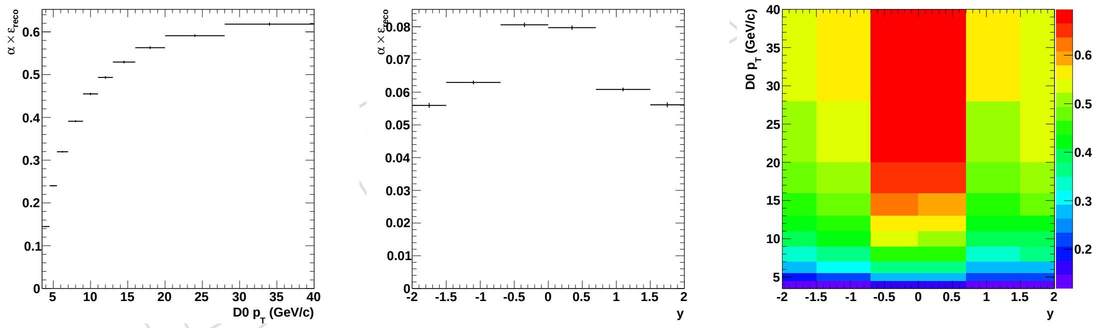

Figure 11: $\alpha \times \epsilon_{reco}$ of prompt D^0 as function of pt and y

6.0.3 D^0 Cuts Selection Efficiency

This subsection provides the estimation of ϵ_{cuts}, which is the D^0 topological cuts efficiency. The formula used is the following:

$$\epsilon_{cuts}(p_T, y) = \frac{N^{MC\ Truth\ Candidate}_{|y|<2.0, p_T^{dau\ track} \geq 1.5, |\eta^{dau\ track}|<2.4, all\ track\ quality\ cuts, all\ D^0\ cuts}}{N^{MC\ Truth\ Candidate}_{|y|<2.0, p_T^{dau\ track} \geq 1.5, |\eta^{dau\ track}|<2.4, all\ track\ quality\ cuts, no\ D^0\ cuts}} \tag{3}$$

Figure 13 and Figure 14 respectively show the ϵ_{cuts} of prompt D^0 and B feed-down D^0 as a function of p_T and y.

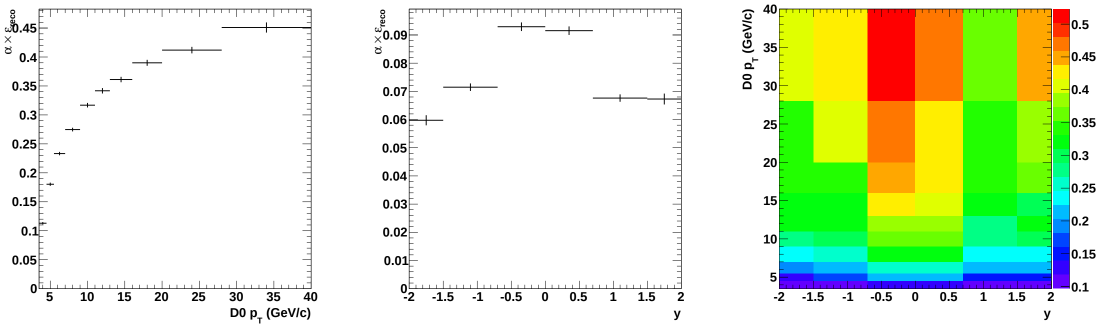

Figure 12: $\alpha \times \epsilon_{reco}$ of B feed-down D^0 as function of pt and y

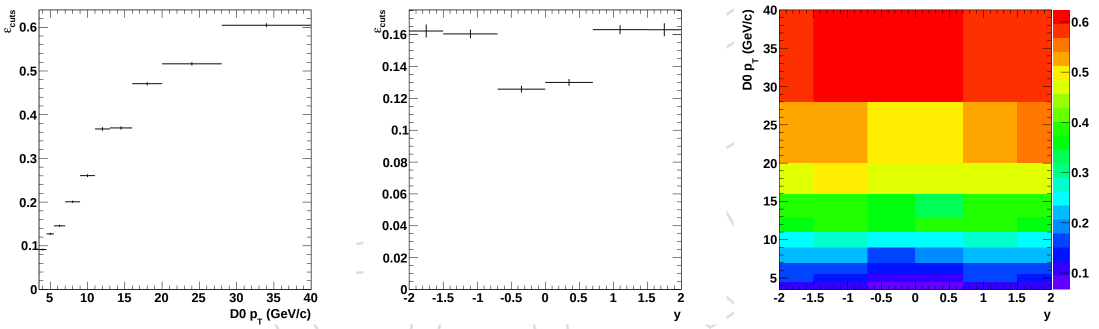

Figure 13: ϵ_{cuts} of prompt D^0 as function of pt and y

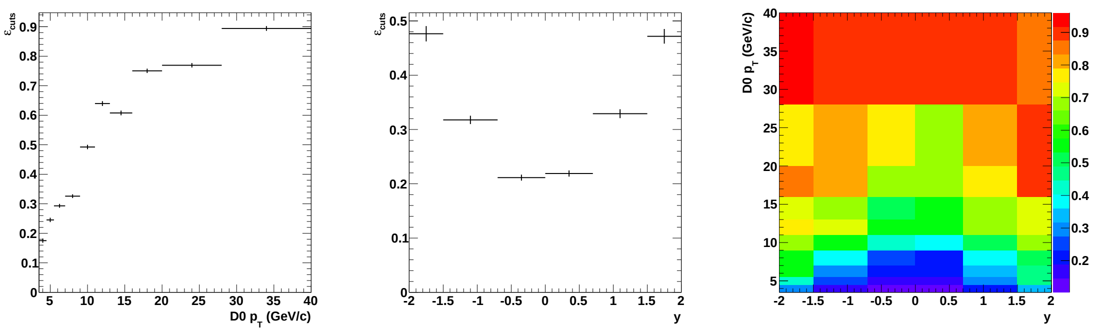

Figure 14: ϵ_{cuts} of B feed-down D^0 as function of pt and y

6.0.4 Match D^0 candidate to generated D^0

In this subsection, the procedure of matching D^0 candidate to generated D^0 is discussed. The procedure is as followed:

- Match daughter tracks of D^0 candidate to TrackingParticle with ”TrackAssociator-ByHits”.
- Mach each trackingparticle to generated particle with p_T, η and ϕ information.
- After above two steps, the match from tracks to generated particles is built. With decay chain information from generated particles, we will able to decide if the two daughter tracks in one D^0 candidate are from same real D^0 decay and if the two tracks are assumed to be right particle identities.
- If the two tracks are from same real D^0 decay and are assumed to be right particle identities, the D^0 candidate is a MC Truth Candidate. If the two tracks are from same real D^0 decay and are assumed to be wrong identities, the D^0 candidate is a particle misidentification D^0. Otherwise, the D^0 candidate is background.

Figure 15 and Figure 16 show the maching performance. From Figure 15, the p_T difference between MC Truth Candidate and matched generated D^0 is mostly smaller than 0.3 GeV/c and pt resolution is smaller than 3%. From Figure 16, the ΔR ($\sqrt{\Delta\eta^2 + \Delta\phi^2}$) between MC Truth Candidate and matched generated D^0 is smaller than 0.01. So our p_T and position resolution of D^0 is pretty good.

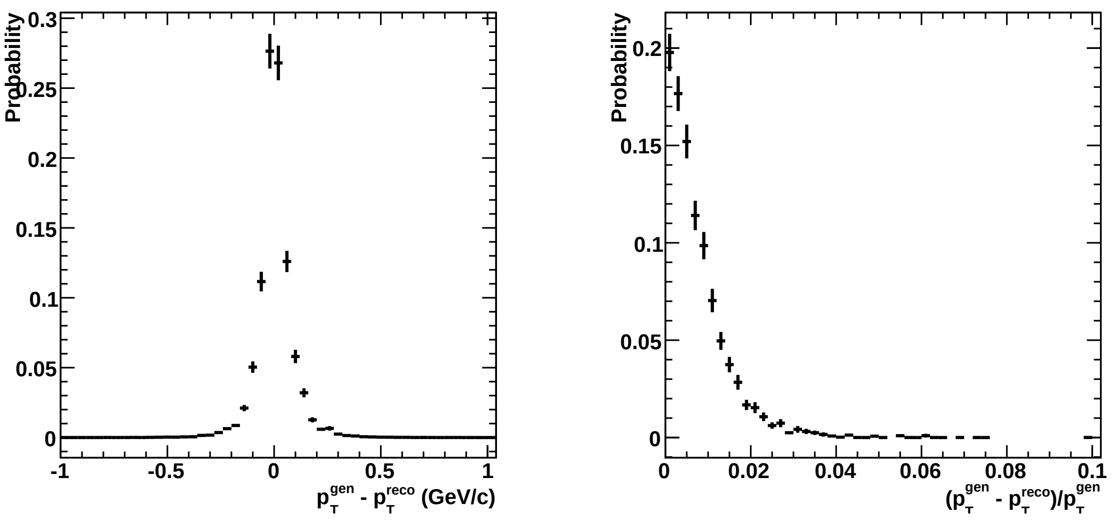

Figure 15: p_T difference between MC Truth Candidate and matched generated D^0

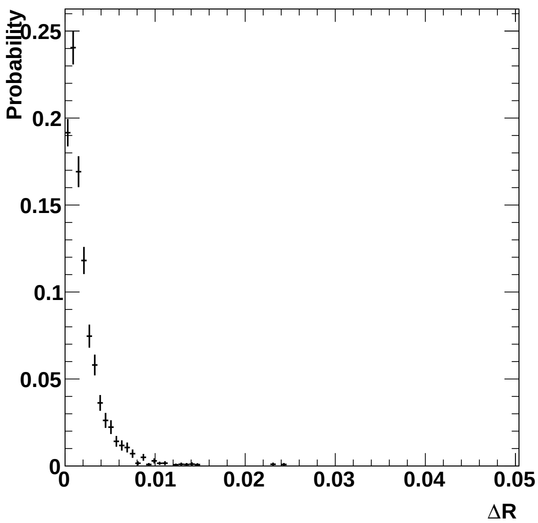

Figure 16: ΔR between MC Truth Candidate and matched generated D^0

7 B Feed-down correction

8 Proton-proton reference

9 Results

In this section, the prompt D^0 spectra and RAA in several different centrality bins is showed. The prompt D^0 spectra in PbPb collision is calculated as following:

$$\frac{dN_{PbPb}}{dp_{\mathrm{T}}} = \frac{f_{prompt} \cdot \frac{1}{2} N^{raw}_{PbPb}}{\Delta p_{\mathrm{T}}} \cdot \frac{1}{N_{\mathrm{MB}} \cdot Br \cdot (\alpha \times \varepsilon)_{prompt}} \tag{4}$$

And the prompt D^0 RAA is calculated as following:

$$R_{AA} = \frac{1}{T_{AA}} \frac{\frac{dN_{PbPb}}{dp_{\mathrm{T}}}}{\frac{d\sigma_{pp}}{dp_{\mathrm{T}}}} \tag{5}$$

The The ingredients entering above two equations are:

- f_{prompt} is the fraction of prompt D^0, discussed in Section 7;
- N_{PbPb} is the raw number of D^0 and $\bar{D}^0$ from mass spectrum fit in PbPb collisions, discussed in Section 5;
- $\frac{1}{2}$ is because what got from fit is the total number of D^0 and $\bar{D}^0$.
- N_{MB} is the number of minimum bias events sampled by the event selection;
- Br is the branching fration of $D^0 \to K^- \pi^+$, which is $3.88 \pm 0.05\%$.
- $(\alpha \times \varepsilon)_{prompt}$ is the prompt D^0 acceptance and efficiency in PbPb collisions, discussed in Section 6;
- T_{AA} is the nuclear overlap function which varies with the centrality, showed in Tab. 6;
- $\frac{d\sigma_{pp}}{dp_{\mathrm{T}}}$ is the prompt D^0 p_{T}-differential cross section from FONLL calculation, discussed in Section 8.

10 Systematics

In this section, checks and systematic uncertainty studies are presented.

10.1 Overall scale related to the cross-section calculation

There are two dominant source of systematics in this category: (1) TAA from Glauber model (2) Exclusive D^0 decay chain branching fractions

10.1.1 TAA Uncertainty

The TAA values and uncertainties are taken from AN-2010/412. They are showd in Tab. 6.

10.1.2 Branching fraction

From PDG, the braching fraction of $\mathrm{D}^0 \rightarrow K^- \pi^+$ is $3.88 \pm 0.05\%$. The relative uncertainty is 1.29%.

10.2 Systematics related to track reconstruction

10.3 Systematics related to D^0 meson selection, efficiency correction

10.3.1 Undertainty due to p_T shape

The FONLL spectrum cannot describe the data perfectly and there is RAA in data, which will lead to the efficiency correction we get with FONLL spectrum as input may not be the same with the efficiency correction in data. A specific uncertainty due to the p_T shape needs to be assigned. Figure 17 shows preliminary prompt D^0 RAA and the RAA is fit with a second order polynomial. To correct p_T spectrum in simulation, we reweight the p_T spectrum in simulation with the fitted second order polynomial on the top of FONLL p_T spectrum weight, which means we first weight the raw p_T spectrum to FONLL p_T spectrum and then weight the spectrum with the fitted second order polynomial.

Figure 18 shows the D^0 uncorrected $\mathrm{dN}/\mathrm{d}p_\mathrm{T}$ with analysis cuts in data and simulation without RAA reweight (left) and with RAA reweight (right). The total yield in simulation is scaled to the total yield in data. From the plots, it is clear that, with RAA reweight, the uncorrected $\mathrm{dN}/\mathrm{d}p_\mathrm{T}$ in simulation is more close to the uncorrected $\mathrm{dN}/\mathrm{d}p_\mathrm{T}$ in data than without RAA reweight though there are still some differences.

Figure 19 shows prompt D^0 acceptance and efficiency without RAA reweight and with RAA reweight in 0-100% centrality. From the plots, the acceptance and efficiency difference between without RAA reweight and with RAA reweight is within 0.5%. We assign 0.5% uncertainty for this.

10.3.2 Further checks on Data and MC cut variable comparison

In Section 4, we discussed the cut variable comparison between Data and MC. We did some futher checks in this section.

First, as discussed in Section 10.3.1, there is difference between the uncorrected D^0 p_T spectrum in data and simulation because the FONLL spectrum cannot describe the data perfectly and there is RAA in data. The RAA reweight is applied in simulation to see the influence on cut variable distribution. Figure 20 shows the cut variable comparison of MC Truth prompt D^0 in simulation without the RAA reweight and with RAA reweight with with $p_\mathrm{T} > 3.5\,\mathrm{GeV}/c$. The plots show some differences but the differences are small.

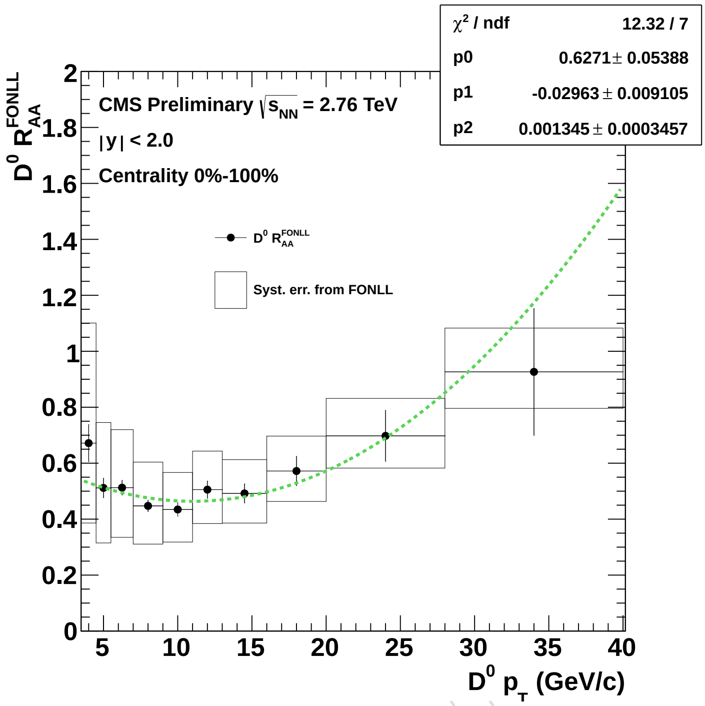

Figure 17: D^0 RAA in 0-100% centrality with statistical error and systematic error from FONLL. The RAA is fit with a second order polynomial.

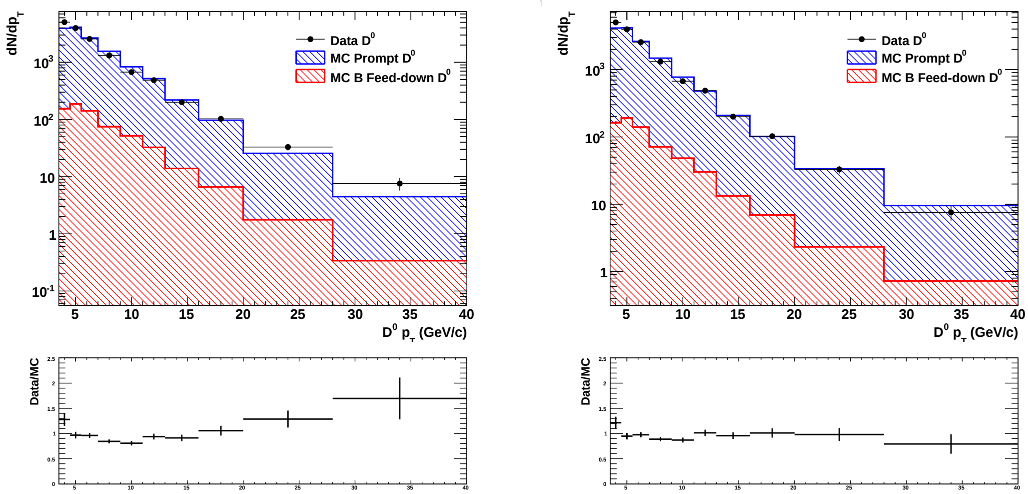

Figure 18: D^0 uncorrected dN/dp_T with analysis cuts in data and simulation without RAA reweight (left) and with RAA reweight (right). The ratio is also showed.

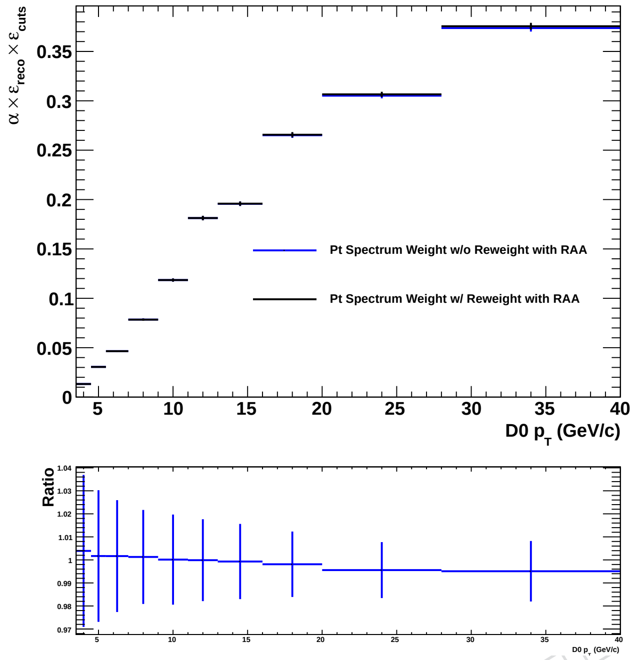

Figure 19: Prompt D^0 acceptance and efficiency without RAA reweight and with RAA reweight in 0-100% centrality.

Second, in simulation, we compared the distributions from sideband method with distributions of MC Truth D^0 to have a look at the sideband method performance. Figure 21 shows the variable comparison of prompt D^0 from sideband method and MC Truth D^0 in simulation with $p_T > 7.0\,\mathrm{GeV}/c$. From the plots, we can see there are some differences between the distributions from sideband method and distribtions of MC truth D^0. We apply the sideband method to both data and MC. And we suppose the sideband method affects the distribions in data and MC in the same way.

Third, we compared the variable distributions with sideband method in Data with distributions of the MC truth D^0. Figure 22 shows this cut variable comparison with $p_T > 7.0\,\mathrm{GeV}/c$. Compared with Figure 2, Figure 22 shows better agreement between data and simulation, which means the distributions with sideband method in data agree better with distributions from MC truth D^0 than distributions with sideband method in simulation. This may suggest the sideband method affects the signal distributions got from data and mc slightly differently. In simulation, we did not model the background correctly, which is pretty difficult . This may lead to the sideband method affects the signal distributions differently in data and MC. But this effect is difficult to evaluate presently. To be consistent, we still use the variable distributions with sideband method in simulation to evaluate the efficiency correction uncertatinty in the following section.

In summary, the RAA reweight on the p_T spectrum in simulation has small influence on the cut variable distributions. There is some clue showing that the sideband method may affect the distributions in data and simulation differently, but it is difficult to evaluate and we still decide to apply sideband methods to both data and simulation. To take the influence of p_T spectrum into account, we compared the the cut variable distributions with sideband method in data and simulation with RAA reweight applied in simulation. Figure 23 shows the comparison plots with RAA reweight applied in simulation. There is small difference between Figure 2 and

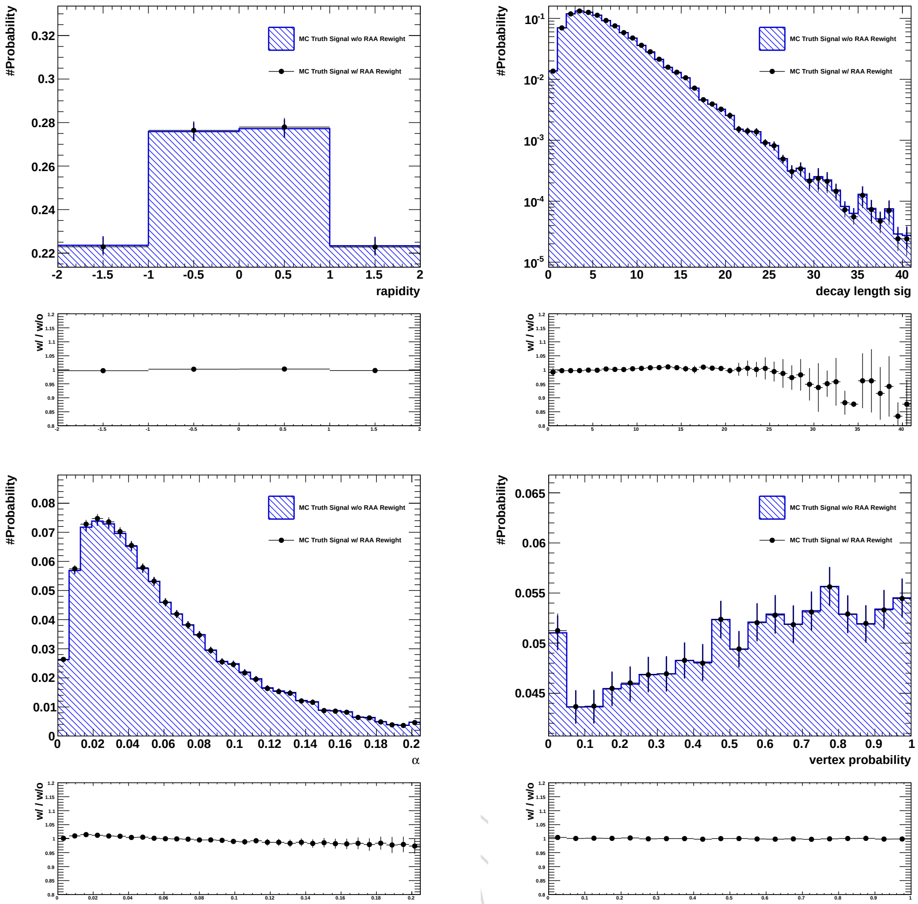

Figure 20: Distributions of rapidity, *d0/d0Err*, α and vertex probability for MC Truth prompt D^0 in simulation without RAA reweight and with RAA reweight with $p_{\mathrm{T}} > 3.5\,\mathrm{GeV}/c$

Figure 23 as expected.

10.3.3 Systematic uncertainty on cut efficiency

A non perfect agreement between the cut variable distributions of D^0 signal in data and MC simulation can eventually introduce a bias in the cross section measurement and thus in the nuclear modification factor. To evaluate this effect, a specific systematic uncertainty was evaluated. The uncertainty estimate is based on the cut variable comparison plots in Figure 23. With the distributions, we computed the following ratio for each selection variable i:

$$Ratio(Data/MC)(i) = \frac{\frac{Yield^i_{Data}(cut)}{Yield^i_{Data}(nocut)}}{\frac{Yield^i_{MC}(cut)}{Yield^i_{MC}(nocut)}} \tag{6}$$

where $Yield^i_{Data}(cut)$ and $Yield^i_{Data}(nocut)$ are from the integral of variable distribion of data D^0 signal for variable i as showed in Figure 23. Similarly for $Yield^i_{MC}(cut)$ and $Yield^i_{MC}(nocut)$.

As discussed in Section 4, when we study variable i, cuts on other variables (d0/d0error > 3.5, $\alpha < 0.05$ and vertex probability > 0.05) are applied.

Based on Tab. 3, 4 and 5, for $p_{\mathrm{T}} > 7.0\,\mathrm{GeV}/c$ D^0, efficiency correction uncertainties due to *d0/d0Err*, α and vertex probability are $11.2\%, 8.0\% and 1.1\%$ respectively. And the total uncertat-

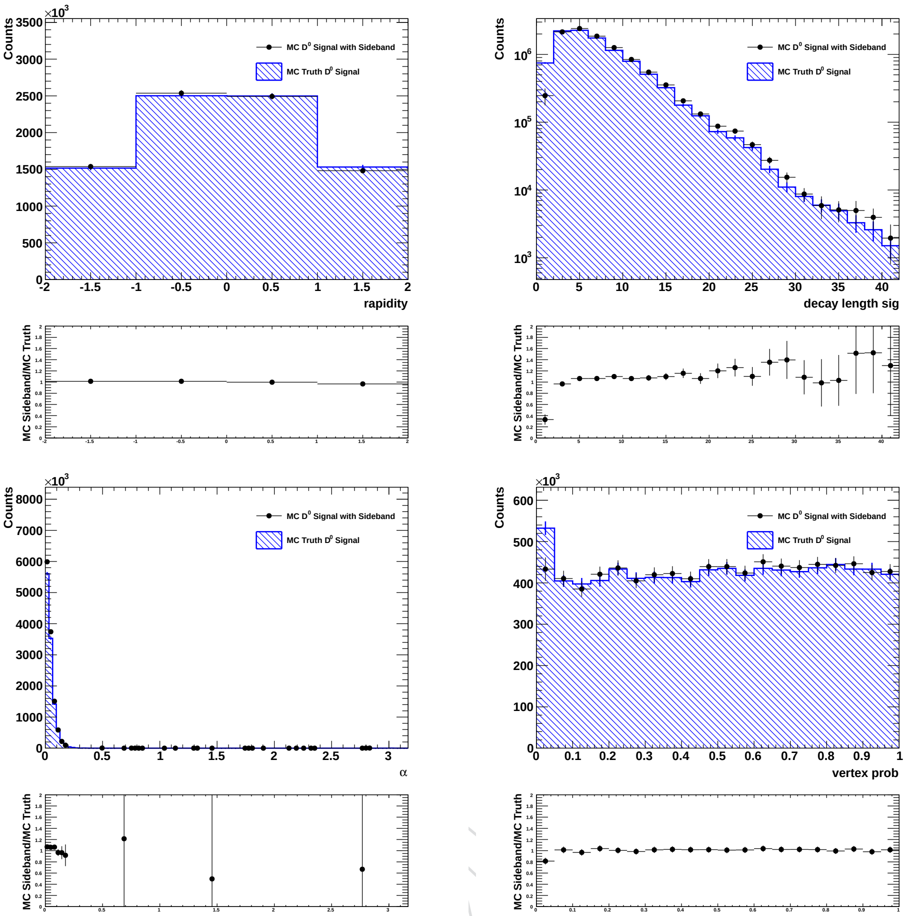

Figure 21: Distributions of rapidity, *d0/d0Err*, α and vertex probability for prompt D^0 from sideband method and MC Truth D^0 in simulation with $p_{\mathrm{T}} > 7.0\,\mathrm{GeV}/c$.

inty due to the cut variables is 13.8%. As discussed in Section 10.3.2, it is possible that sideband method has different influences on variable distributions in data and simulation, which may be the reason of this big uncertainty. And if we use variable distributions in Figure 22, the uncertainty will be much smaller.

Cut on *d0/d0Err*	$Yield^i_{Data}(cut)/Yield^i_{Data}(nocut)$	$Yield^i_{MC}(cut)/Yield^i_{MC}(nocut)$	Ratio (Data/MC)
3.0	0.839 ± 0.043	0.893 ± 0.007	0.940 ± 0.049
3.5	0.778 ± 0.041	0.838 ± 0.007	0.929 ± 0.049
4.0	0.700 ± 0.037	0.778 ± 0.006	0.899 ± 0.048
4.5	0.638 ± 0.034	0.719 ± 0.006	0.888 ± 0.048

Table 3: Double ratios obtained with different *d0/d0Err* cuts

10.3.4 p_{T} resolution correction

As showed in Section 6.0.4, we have pretty good D^0 p_{T} resoultion, smaller than 3%. Here we checked p_{T} resoultion effect with signal MC by comparing the reconstructed and generated p_{T} sepectra of D^0. The effect of p_{T} resolution correction is very small. We put 3.0% as the maximum value Figure 24 shows the effect of p_{T} resolution correction for D^0.

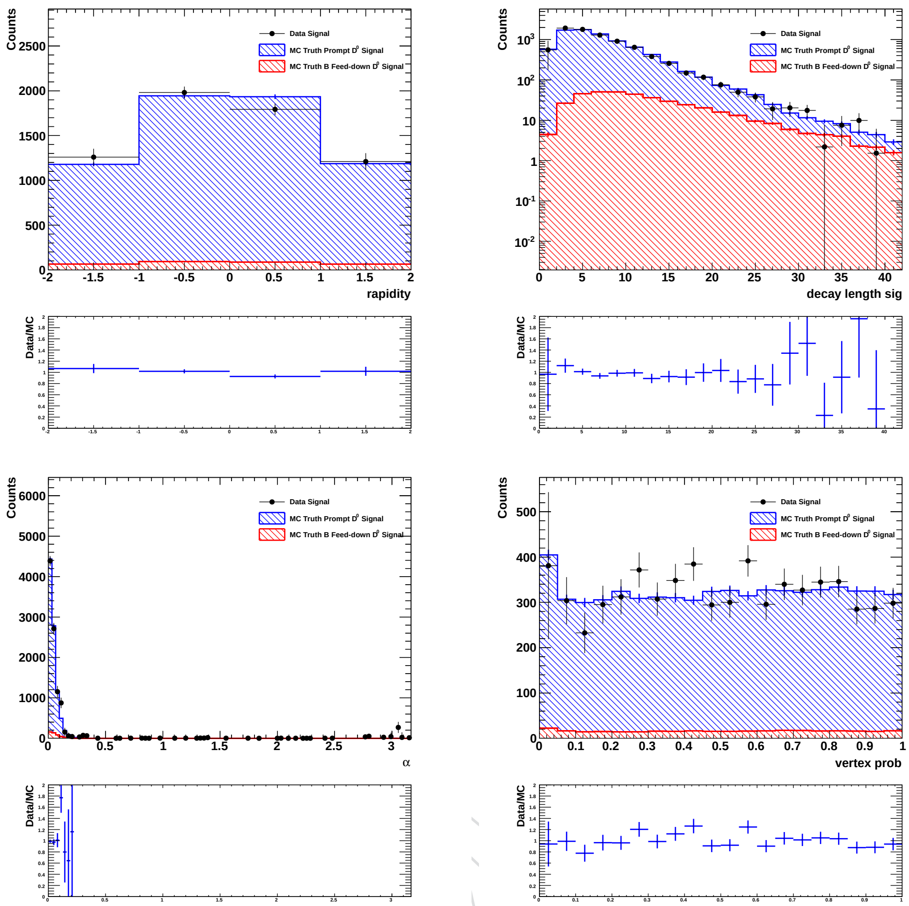

Figure 22: Distributions of rapidity, *d0/d0Err*, α, α zoomed in to range [0, 0.1] and vertex probability for D^0 signals from data and MC simulation with $p_{\mathrm{T}} > 7.0\,\mathrm{GeV}/c$. Data distributions are from sideband method and MC distributions are from MC truth D^0

Cut on α	$Yield^i_{Data}(cut)/Yield^i_{Data}(nocut)$	$Yield^i_{MC}(cut)/Yield^i_{MC}(nocut)$	Ratio (Data/MC)
0.15	1.000 ± 0.000	1.000 ± 0.000	1.000 ± 0.000
0.10	0.904 ± 0.037	0.978 ± 0.006	0.925 ± 0.038
0.07	0.800 ± 0.035	0.870 ± 0.006	0.920 ± 0.041
0.05	0.692 ± 0.032	0.734 ± 0.006	0.944 ± 0.043

Table 4: Double ratios obtained with different α cuts

10.3.5 Check with Pthat weight

As discussed in Section 6, to get the acceptance and efficiency correction, the raw p_{T} spectrum in simulation is weighted to FONLL spectrum. However, D^0 from different pthat events may have sightly different efficiency correction because the surroundings may affect the reconstruction performance. For example, construction performance of D^0 in high pt Jet may be affected by the tracks around, but standalone D^0 will not be affected by the surroundings. To check this, we compared D^0 efficiency corrections from pthat weight method with efficiency corrections from our pt spectrum weight method. Pthat weight is based on the crosssection and filter efficiency, which should reproduce pythia minbias D^0 surroundings. We don't use pthat weight method as our default method because it requires big statistics to get small statistical error and the surroundings influence on D^0 reconstruction performance is expected to be small. To evaluate this uncertainty, we need to evaluate the difference of $\alpha \times \epsilon_{reco}$ with FONLL p_{T} spectrum

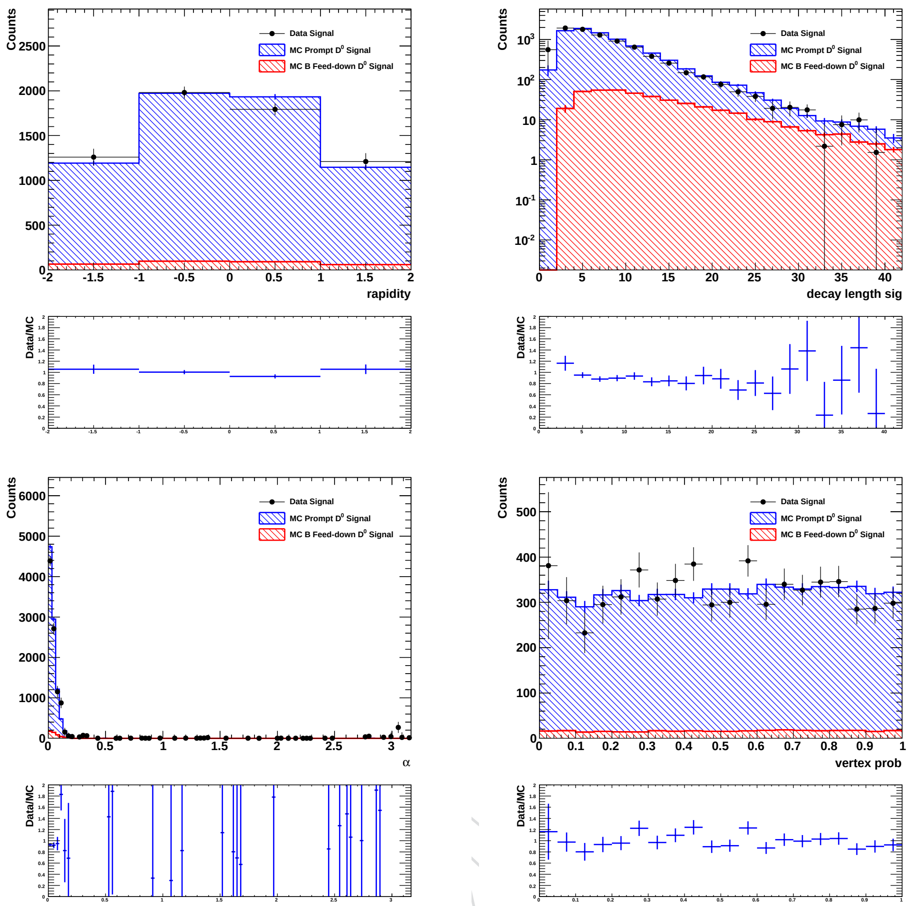

Figure 23: Distributions of rapidity, *d0/d0Err*, α, α zoomed in to range [0, 0.1] and vertex probability for D^0 signals from data and MC simulation with $p_T > 7.0\,\mathrm{GeV}/c$. Sideband method is used in both data and simulation. And the RAA reweight on the p_T spectrum is applied in simulation

Cut on vertex prob	$Yield^i_{Data}(cut)/Yield^i_{Data}(nocut)$	$Yield^i_{MC}(cut)/Yield^i_{MC}(nocut)$	Ratio (Data/MC)
0.05	0.940 ± 0.024	0.949 ± 0.003	0.991 ± 0.025
0.08	0.912 ± 0.024	0.922 ± 0.003	0.989 ± 0.026
0.10	0.894 ± 0.024	0.901 ± 0.004	0.992 ± 0.027
0.15	0.858 ± 0.024	0.856 ± 0.004	1.001 ± 0.028

Table 5: Double ratios obtained with different vertex probability cuts

weight and pthat weight. We should take the difference of ϵ_{cuts} into the uncertainty because we have evaluated the uncertainty due to cut variable difference between data and simulation with p_T spectrum weight in Section 10.3.3.

Figure 25 shows prompt D^0 $\alpha \times \epsilon_{reco}$ with FONLL p_T spectrum weight and pthat weight. The difference is within 3.5%. Figure 26 shows prompt D^0 $\alpha \times \epsilon_{reco}$ in pthat 0 to 30 and 30 above events and pretty small difference is observed. Based on this, 3.5% uncertainty is assigned.

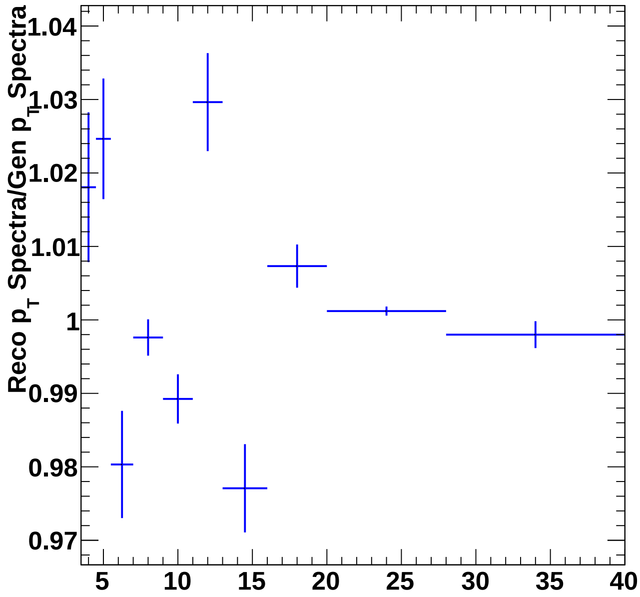

Figure 24: The effect of p_{T} resolution correction for D^0

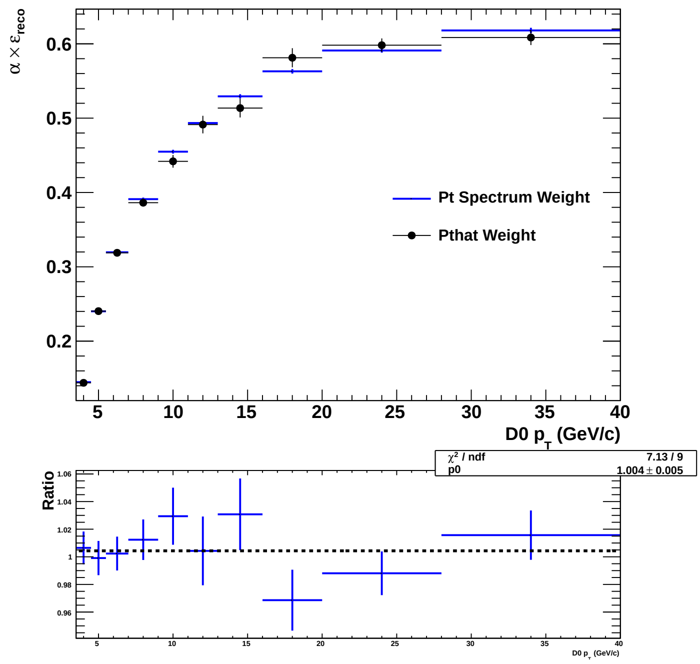

Figure 25: Prompt D^0 $\alpha \times \epsilon_{reco}$ with FONLL p_{T} spectrum weight and pthat weight.

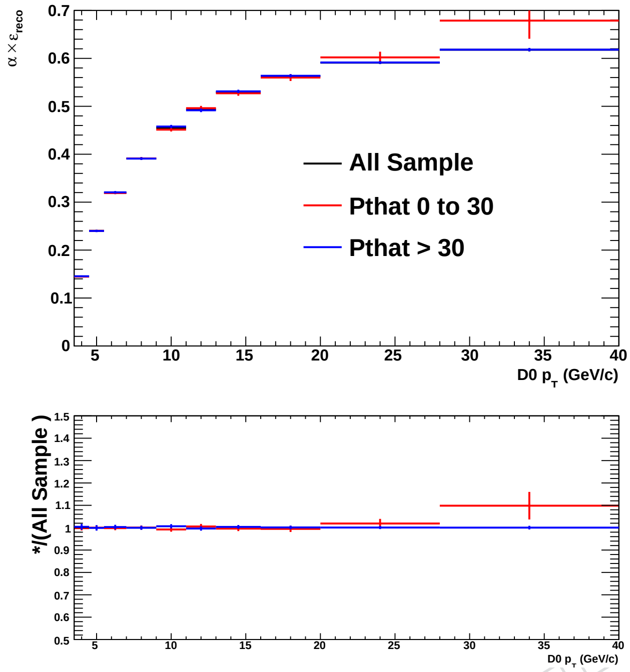

Figure 26: Prompt D^0 $\alpha \times \epsilon_{reco}$ in pthat 0 to 30 and 30 above events.

10.4 Systematic associated with signal extraction fit

10.4.1 Particle misidentification D^0

As discussed in Section 5.2, there is no PID on each single track, so K and π tracks from real D^0 may form two D^0 candidates (Kπ and πK). And from Figure 7, the D^0 candidates with daughter tracks misidentification (gray open circles) have broad guassian mass distribution, which may introduce bias to the signal extraction. A specific uncertainty due to the particle misidentification D^0 should be studied and assigned. The procedure is as followed

- First, the invariant mass of particle misidentification D^0 candidates in bins of D^0 p_T is fitted with Gaussian function, showed in Figure 28. The gray open circles are the mass distributions and the gray dashed lines are fitted results.
- Second, the fitted results in simulation are used to evaluate the particle misidentification D^0 candidates in data. The D^0 candiate mass spectrum in data is fitted with the fit function composed of a Gaussian for D^0 signal, a second order polynomial for the background and another Gaussian for the particle misidentification D^0 candidates. The parameters of the Gaussian for the particle misidentification D^0 candidates are fixed to the parameters got from simulation with scaling by some factors to match the fitted D^0 signal yield.
- The D^0 raw yield differences from the default fit and fit discussed above with fixed particle misidentification D^0 candidates shape are evaluated in different p_T bins and the uncertainties are assigned based on the differences. Figure 29 shows the D^0 raw yield and ratio with default fit and fit with fixed particle misidentification D^0 candidates shape. Due to the peak structure of particle misidentification D^0, the default fit tends to overevaluate the D^0 yield. Based on the ratio plot, the asymmetric uncertainties are assigned to be $^{+0.0}_{-9.0}$% for p_T 3.5 GeV to 4.5 GeV, $^{+0.0}_{-5.0}$% for p_T 4.5 GeV to 7.0 GeV, and $^{+0.0}_{-2.0}$% for p_T 7.0 GeV to 40 GeV.

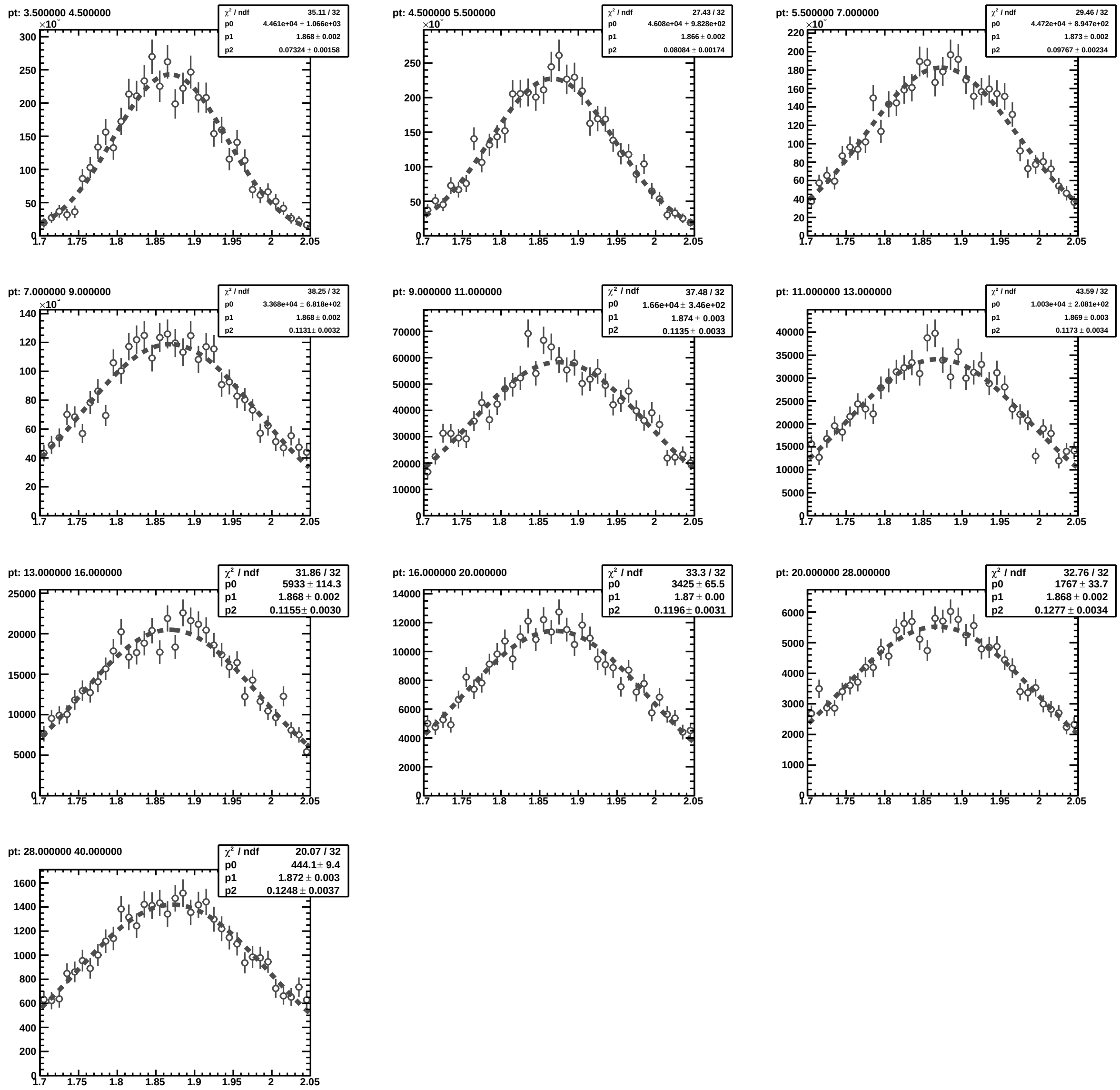

Figure 27: Invariant mass fit of particle misidentification D^0 candidates in bins of D^0 p_T in simulation

400 ## 10.5 Systematics related to B feed down correction

401 ## 10.6 Systematics related to the theoretical reference

402 ## 10.7 Summary of systematics

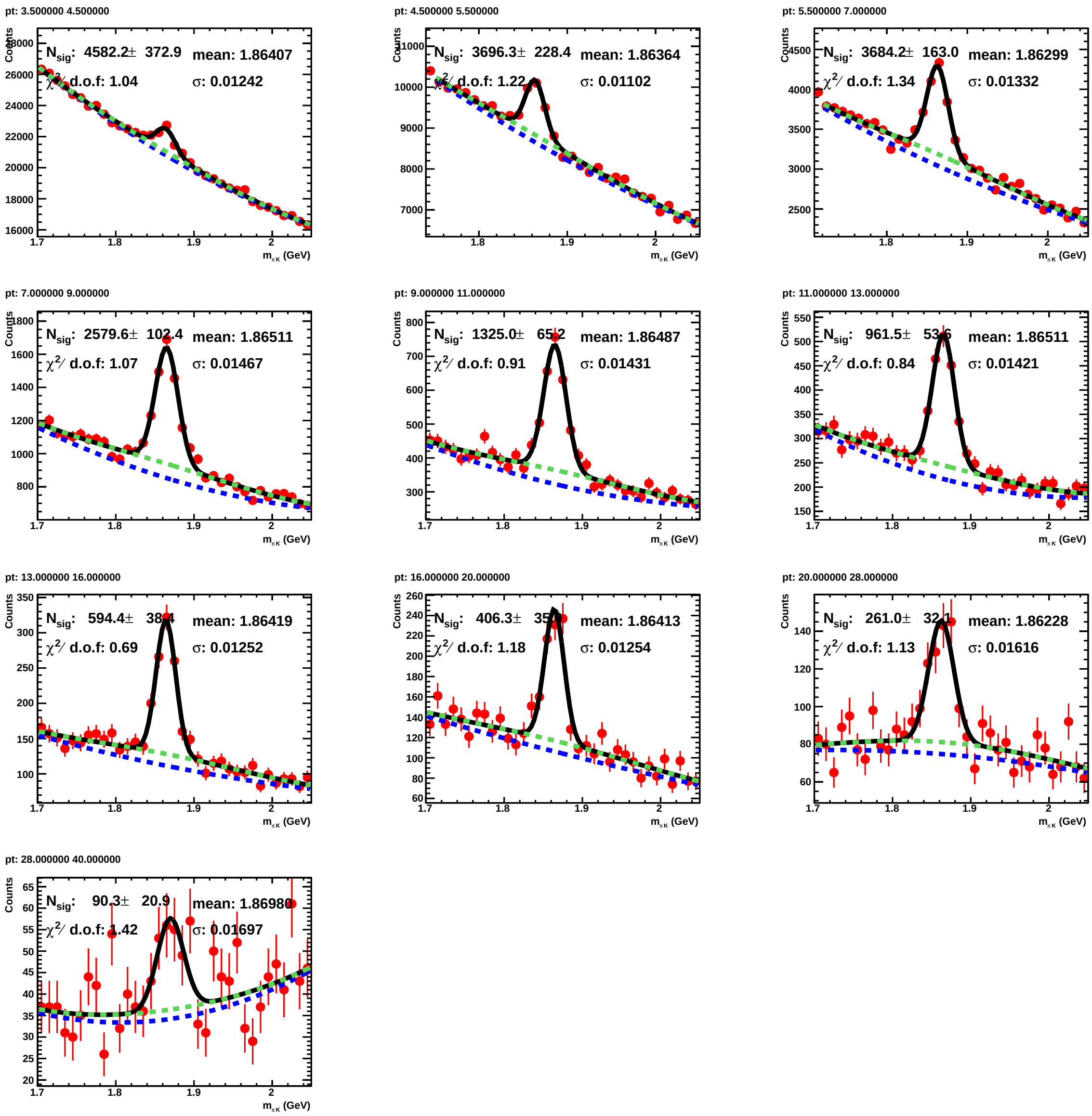

Figure 28: Invariant mass fit of D^0 candidates in bins of D^0 p_T in data. The fit function is composed of a Gaussian for D^0 signal, a second order polynomial for the background and another Gaussian for the particle misidentification D^0 candidates. The black lines are the fitted results. The green dashed lines are the second order polynomial for the background plus the Gaussian for the particle misidentification D^0 candidates. And the blue dashed lines are the second order polynomial for the background. So the difference between the green dashed lines and the blue dashed lines are Gaussian for the particle misidentification D^0 candidates.

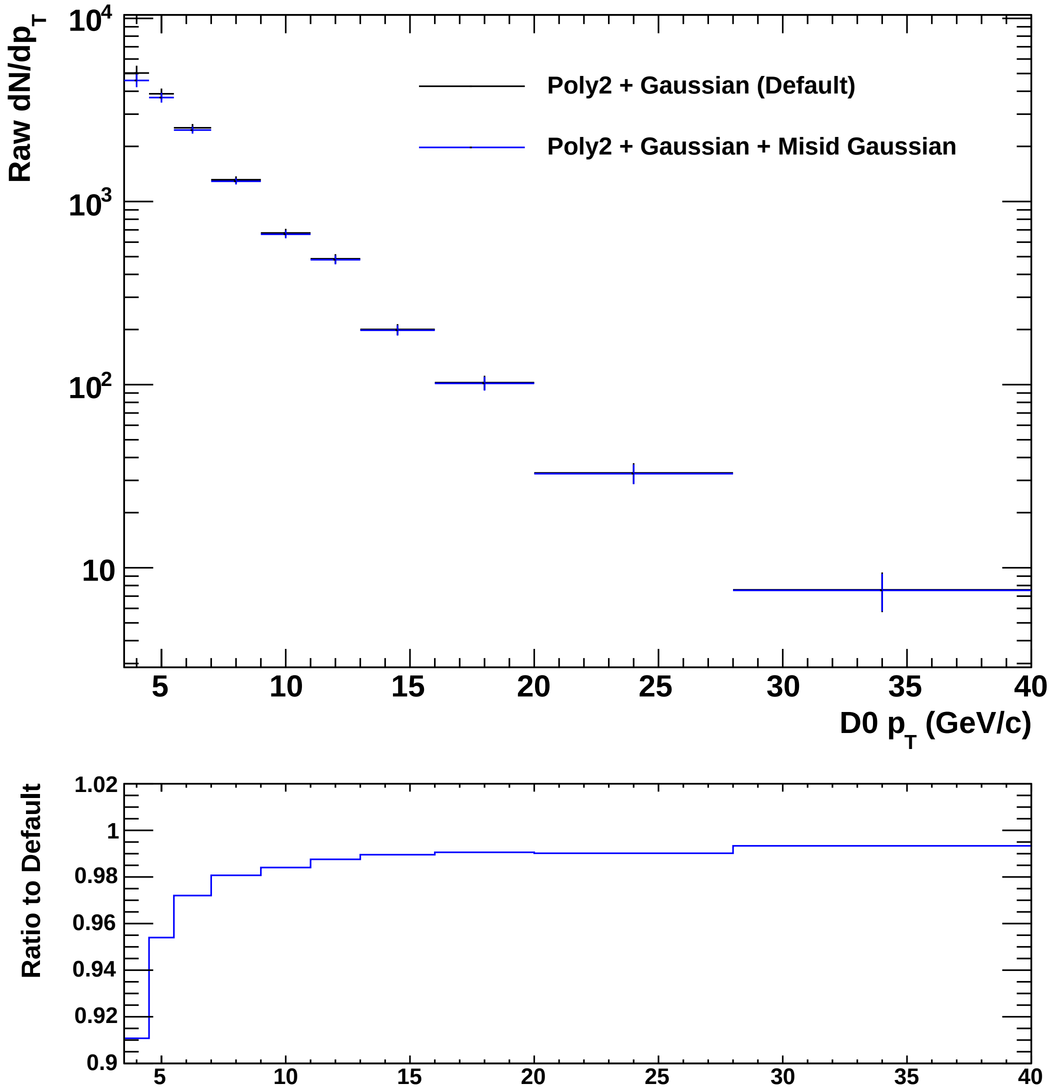

Figure 29: D^0 raw yield and yield ratio with default fit and fit with fixed particle misidentification D^0 candidates shape

11 Conclusions

A Appendix

A.1 TAA for different centrality bins

Table 6: Glauber model results from AN-2010/412

centrality	$< N_{\text{part}} >$	N_{part} RMS	$< T_{AA} >$ (1/mbarn)	T_{AA} RMS
0 - 10%	355.45±2.83(0.8%)	33.34	23.20±0.99(4.3%)	3.77
0 - 20%	308.47±2.86(0.9%)	56.79	18.84±0.85(4.5%)	5.49
10 - 30%	224.42±4.17(1.9%)	45.93	11.64±0.67(5.7%)	3.75
30 - 50%	108.15±4.47(4.1%)	27.06	3.92±0.37(9.3%)	1.58
30 - 100%	46.65±2.73(5.9%)	44.57	1.45±0.15(10.5%)	1.83
50 - 100%	22.06±1.16(5.3%)	19.26	0.47±0.05(11.1%)	0.54
0 - 100%	113.09±2.92(2.6%)	115.61	5.67±0.32(5.7%)	7.54

A.2 Variable comparison between prompt and B feed-down D^0

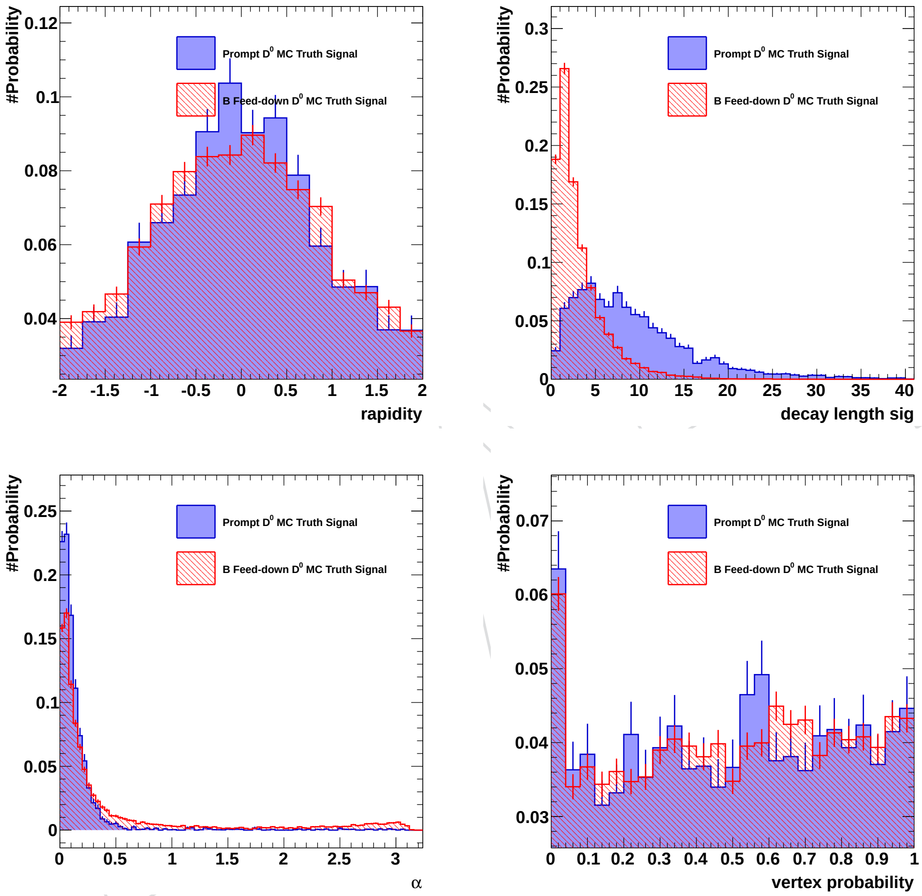

Figure 30: Variable distributions of prompt and B feed-down D^0

References

[1] N. Armesto *et.al.*, "Heavy-ion collisions at the LHC-Last call for predictions", *J. Phys. G 35*,.

[2] CMS Collaboration, "Prompt and non-ptompt $J/\psi R_{AA}$ with 150 μb^{-1} integrated PbPb luminosity at $\sqrt{s_{NN}} = 2.76$ TeV", *CMS PAS HIN-12-014* (2012).

[3] CMS Collaboration, "Measurement of the $B^{+}, B^{0} and B_{s}^{0} production cross sections in pPb collisions at \sqrt{s_{NN}} = 5.02$ TeV", *CMS PAS HIN-14-004* (2014).

[4] CMS Collaboration, "Nuclear modification factor R_{pA} of b jets in pPb collisions", *CMS PAS HIN-14-007* (2014).

[5] M. Cacciari, M. Greco, P. Nason, "The p_T Spectrum in Heavy-Flavour Hadroproduction", *JHEP 007,* **9805** (1998).

[6] CMS Collaboration, "The CMS experiment at the CERN LHC", *JINST* **S08004** (2008).

[7] CMS Collaboration, "Azimuthal anisotropy of charged hadrons at high transverse momentum in PbPb collisions at $\sqrt{s_{NN}}$ = 2.76 TeV", CMS Analysis Note AN-11-436, CMS, 2012.

[8] CMS, "Observation and studies of jet quenching in PbPb collisions at $\sqrt{s_{NN}} = 2.76$ TeV", *Phys. Rev. C* (2011) `arXiv:1102.1957`.

[9] CMS Collaboration, "Gamma-jet correlation studies in PbPb collisions", CMS Analysis Note AN-11-435, CMS, 2012.

[10] CMS Collaboration, "Energy loss in high transverse momentum dijets in PbPb collisions at nucleon-nucleon center-of-mass energy = 2.76 TeV", CMS Analysis Note AN-11-478, CMS, 2012.

[11] CMS Collaboration, "Measurement of jet fragmentation functions in central PbPb collisions at 2.76 TeV", CMS Analysis Note AN-11-121, CMS, 2012.

[12] CMS Collaboration, "Centrality dependence of dijet energy balance distributions in PbPb collisions at 2.76 TeV", CMS Analysis Note CMS-AN-10-399, CMS, 2011.

[13] CMS Collaboration, "Studies of jet quenching using isolated-photon+jet correlations in PbPb and pp collisions at $\sqrt{s_{NN}}$ = 2.76 TeV", `arXiv:1205.0206`.

[14] CMS Collaboration, "Jet momentum dependence of jet quenching in PbPb collisions at $\sqrt{s_{NN}}$=2.76 TeV", `arXiv:1202.5022`.

[15] CMS Collaboration, "Measurement of jet fragmentation into charged particles in pp and PbPb collisions at $\sqrt{s_{NN}}$= 2.76 TeV", `arXiv:1205.5872`.

[16] CMS Collaboration, "Observation and studies of jet quenching in PbPb collisions at $\sqrt{s_{NN}}$=2.76 TeV", *Phys. Rev. C* **84** (2011) 024906, `doi:10.1103/PhysRevC.84.024906`, `arXiv:1102.1957`.

[17] D. Lange, "The EvtGen particle decay simulation package", *Nucl.Instrum.Meth.* **A462** (2001) 152–155, `doi:10.1016/S0168-9002(01)00089-4`.

[18] E. Barberio, B. van Eijk, and Z. Was, "PHOTOS: A Universal Monte Carlo for QED radiative corrections in decays", *Comput.Phys.Commun.* **66** (1991) 115–128, doi:10.1016/0010-4655(91)90012-A.